

## REVIEW

## The Hadley circulation in a changing climate

Piero Lionello<sup>1</sup>  | Roberta D'Agostino<sup>2,3</sup> | David Ferreira<sup>4</sup> | Hanh Nguyen<sup>5</sup> | Martin S. Singh<sup>6</sup>

<sup>1</sup>DiSteBA - Dipartimento di Scienze e Tecnologie Biologiche e Ambientali, University of Salento, Lecce, Italy

<sup>2</sup>Max-Planck-Institut für Meteorologie, Hamburg, Germany

<sup>3</sup>National Research Council, Institute of Atmospheric Sciences and Climate, Lecce, Italy

<sup>4</sup>Department of Meteorology, University of Reading, Reading, UK

<sup>5</sup>Bureau of Meteorology, Melbourne, Victoria, Australia

<sup>6</sup>School of Earth, Atmosphere, and Environment, Monash University, Melbourne, Victoria, Australia

## Correspondence

Piero Lionello, DiSteBA - Dipartimento di Scienze e Tecnologie Biologiche e Ambientali, University of Salento, via per Monteroni 165, 73100 Lecce, Italy.  
Email: [piero.lionello@unisalento.it](mailto:piero.lionello@unisalento.it)

## Funding information

Deutsche Forschungsgemeinschaft, Grant/Award Number: 390683824; Australian Research Council, Grant/Award Numbers: DE190100866, DP200102954, CE170100023; Italian Ministry of University and Research, Grant/Award Number: P2022A3MFC

## Abstract

The Hadley circulation (HC) is a global-scale atmospheric feature with air descending in the subtropics and ascending in the tropics, which plays a fundamental role in Earth's climate because it transports energy polewards and moisture equatorwards. Theoretically, as a consequence of anthropogenic climate change, the HC is expected to expand polewards, while indications on the HC strength are equivocal, as weakening and strengthening are expected in response to different mechanisms. In fact, there is a general agreement among reanalyses and climate simulations that the HC has significantly widened in the last four decades and it will continue widening in the future, but there is no consensus on past and future changes of the HC strength. Substantial uncertainties are produced by the effects of natural variability, structural deficiencies in climate models and reanalyses, and the influence of other forcing factors, such as anthropogenic aerosols, black carbon, and stratospheric and tropospheric ozone. The global HC can be decomposed into three regional HCs, associated with ascending motion above Equatorial Africa, the Maritime Continent, and Equatorial America, which have evolved differently during the last decades. Climate projections suggest a generalized expansion in the Southern Hemisphere, but a complex regional expansion/contraction pattern in the Northern Hemisphere.

## KEYWORDS

climate change, expansion, Hadley circulation, intertropical convergence zone, monsoons, regional Hadley cells, strength

## INTRODUCTION

The Hadley circulation (HC) is a global-scale atmospheric feature that imports moisture in the tropics and exports energy and angular momentum from the tropics to the subtropics, playing a key role in modulating the regional hydrological cycle. The HC consists of two cells, one for each hemisphere, which share an ascending branch in the tropics (the Inter-Tropical Convergence Zone, ITCZ) and have their descending branches in the subtropics. The ascending and descending branches are connected by a flow that in the upper troposphere diverges from the common central ascending branch, exporting energy away from the tropics and in the lower troposphere converges toward the ITCZ, importing moisture.

Variations in the characteristics of the HC are closely associated with those of other global-scale features of the atmospheric circulation, such as monsoons, the mean position of subtropical high pressure systems, the position of jet streams, and the position and intensity of storm tracks. Variations of the HC affect the meridional energy and moisture transport, the tropical and subtropical hydrological cycle, and related precipitation regimes at multiple spatial scales.<sup>1–5</sup> The ascending motion of moist air in the ITCZ is associated with low-level convergence, heavy precipitation, and deep convective systems, and its structural changes affect tropical precipitation maxima and monsoons.<sup>6–8</sup> The descending motion is among the mechanisms determining the low precipitation and arid climates found in the subtropics.<sup>9,10</sup> Consequently, ecosystems, human settlements,

agriculture, and water resources across the tropics and subtropics are potentially affected by variations in the HC, particularly in monsoon regions and vulnerable semi-arid areas, such as the Mediterranean, the southwestern United States and northern Mexico, southern Australia, southern Africa, and parts of South America and it is expected to influence the future evolution of precipitation in many of these semi-arid regions.<sup>11–13</sup>

Historically, the HC was first detected in surface wind maps in the late 17th century by Edmond Halley,<sup>14</sup> who sought to explain the observed surface wind convergence in what is now known as the ITCZ as a result of solar heating in the tropics. About 50 years later, George Hadley<sup>15</sup> applied the concept of momentum conservation to explain the observed westward surface flow characterizing the subtropical trade winds. Though it took about two centuries to fully appreciate the relevance of those studies and to complement surface with upper troposphere observations,<sup>16</sup> the structure of the HC and its dynamics have long been in the background of dynamical meteorology.<sup>17,18</sup> Studies addressing the characteristics of the HC during past climate conditions when the spatial and seasonal distribution of the solar forcing was quite different from the present (typically the last glacial maximum, LGM, ~21 kyr BP, and the mid-Holocene, ~6 kyr BP) date back to the 1950s. The interest of the scientific community was increased in the 1970s, when numerical simulation of the atmospheric circulation became feasible (e.g., Refs. 19–21). In the last few decades, the volume of scientific literature dedicated to studies of the HC has become extremely large (see Refs. 22, 23 for an extensive documentation), and in the 2000s, the effect of anthropogenic greenhouse gas (GHG) on HC has emerged as a major research topic (Refs. 24–27, and subsequent articles cited in this review). Several review papers have been written on the HC (e.g., Refs. 28–32). Though some overlap between this review and others is unavoidable, our paper aims to provide a distinct contribution as it focuses on the underlying theoretical considerations, it discusses in detail the regional characterization of the HC, and it emphasizes both HC width and strength.

The HC is traditionally described using the global Meridional Stream Function  $\Psi(\phi, p)$  [MSF, kg/s, Refs. 33, 34]:

$$\Psi(\phi, p) = \frac{2\pi R_e \cos \phi}{g} \int_0^p v(\phi, p') dp', \quad (1)$$

where  $R_e$  is the Earth's radius,  $\phi$  is latitude,  $g$  is the gravitational acceleration,  $p$  is the atmospheric pressure, and  $v$  is the zonal mean meridional velocity. The global MSF is used to compute properties such as the strength and position of the equatorial ascending branch, the poleward edges of the cells, and the overall HC width. The computation of the MSF using winds provided by profile soundings became possible only in the second half of the 20th century. After preliminary attempts in the 1950s, the first reconstructions were completed in the 1960s,<sup>35,36</sup> and by the 1970s, reconstructions became sufficiently accurate to allow a monthly climatology.<sup>33</sup> In the late 1990s, meteorological reanalyses became available and provided a surrogate of global observations. Instead of using the MSF, some studies have attempted to estimate characteristics and variations of the HC using the sur-

face variables that are affected by it and a variety of different metrics. The HC poleward edges have been identified based on thresholds of the outgoing long-wave radiation,<sup>13,26,37–41</sup> the subtropical absolute precipitation minima,<sup>13,39,42,43</sup> the zero crossing latitude of the precipitation–evaporation imbalance,<sup>13,31,37,38,40,41,44,45</sup> the zonal surface-wind zero crossing,<sup>46</sup> and the subtropical maxima of the mean sea-level pressure.<sup>13,40–42</sup> Proxies of precipitation are often used for geological time scales, including glacial and interglacial cycles and most of the present Holocene epoch (e.g., Ref. 47). However, these variables allow only a partial reconstruction of the full tri-dimensional structure of the HC and some of them poorly correlate with each other.<sup>48,49</sup> Though some metrics, such as the mid-latitude eddy-driven jet, the edge of the subtropical dry zones, and the Southern Hemisphere (SH) subtropical highs exhibit variability and trends consistent with those of the zero crossing latitude of the MSF, others, such as those based on the outgoing longwave radiation, the position of the subtropical jet, the break in the tropopause, and the Northern Hemisphere subtropical highs appear to behave differently.<sup>48</sup> Therefore, metrics other than those based on the MSF are not explicitly considered in this review.

In the annual mean, the global MSF shows two cells, roughly symmetric with respect to the equator, rotating in opposite directions (Figure 1A). This representation corresponds to the transient condition at the equinoxes, while the solstitial condition exhibits one dominant cell extending from the mid-subtropics in the summer hemisphere to the edge of the subtropics in the opposite winter hemisphere (Figure 2, Ref. 50). Furthermore, the HC exhibits pronounced regional variability, as trade winds respond to ocean interbasin thermal and moisture flux contrasts<sup>51–53</sup> and atmospheric flow over land exhibits zonal asymmetries due to surface inhomogeneities and local monsoonal circulations.<sup>53,54</sup> The global MSF is a smoothed result of the superposition of distinct regional meridional overturning circulations that are the consequence of active convection occurring sporadically in time and space in preferred zones.<sup>55,56</sup>

The decomposition of the global MSF into regional components is based on three conceptual steps. The first step is to decompose the horizontal flow at each pressure level  $p$  into divergent and nondivergent components. Second, the divergent flow is further decomposed in a zonal and a meridional component, which are associated with zonally and meridionally oriented overturnings representing the Walker and the HCs, respectively. In fact, the local MSF  $\psi(\lambda, \phi, p)$  can be computed for each longitude  $\lambda$  using the meridional component of the divergent flow  $v_d(\lambda, \phi, p)$  and ensuring mass conservation:

$$\psi(\lambda, \phi, p) = \frac{1}{g} \int_0^p v_d(\lambda, \phi, p') dp', \quad (2)$$

which provides a view of the HC whose strength and edges vary continuously with longitude (e.g., Refs. 13, 57–62). Specifically,  $\psi(\lambda, \phi, p)$  represents a meridional mass flux density, which can be integrated zonally to provide the meridional mass transport across any specified sector. The global MSF can be divided into selected regional MSFs  $\Psi_R(\phi, p)$  by computing the regional zonal average  $v_R(\phi, p)$  of  $v_d$  in

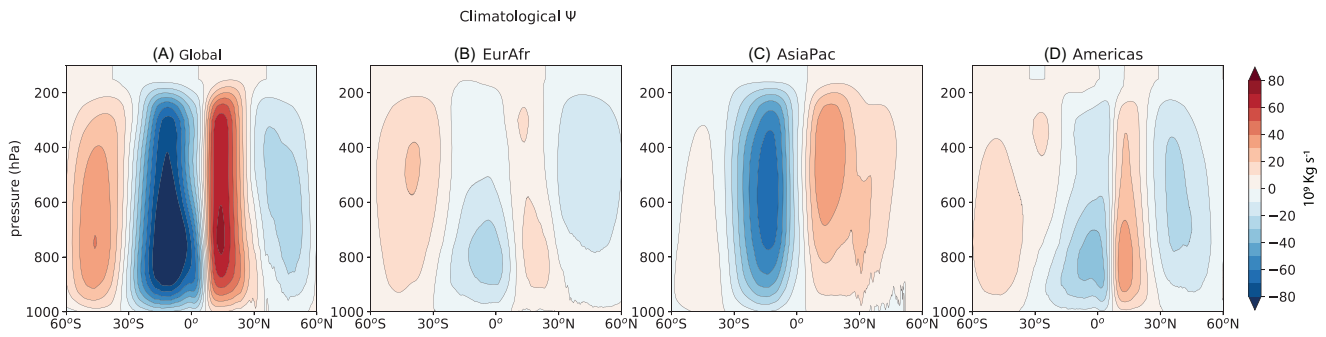


**FIGURE 1** Meridional stream function MSF over the period 1979–2019: global MSF  $\Psi$  (A) and regional MSF  $\Psi_R$  of the Europe-Africa sector (B, EurAfr=20° W–65° E), the Asia-Pacific sector (C, AsiaPac =65° E–140° W), and the sector of the North and South Americas (C, Americas=140° W–20° W). Contour line interval is  $10^{10} \text{ kg} \cdot \text{s}^{-1}$ . All panels are derived from ERA5.<sup>66</sup>

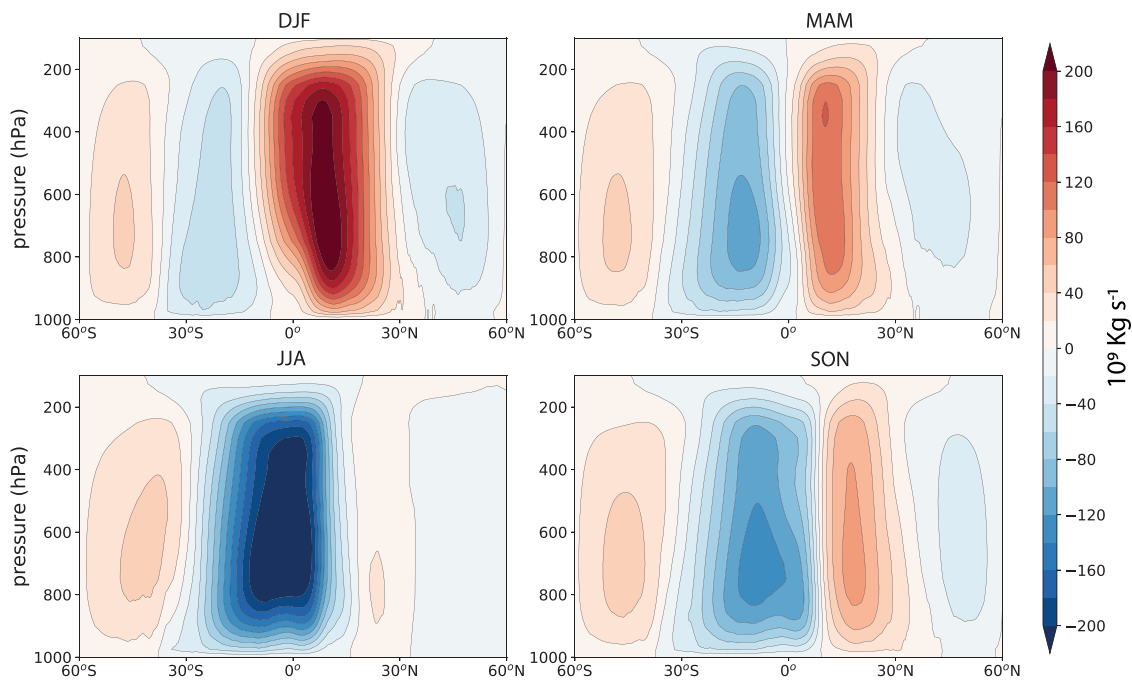


**FIGURE 2** Seasonal cycle of the global MSF over the period 1979–2019 derived from ERA5.<sup>66</sup> Contour line interval is  $2 \cdot 10^{10} \text{ kg} \cdot \text{s}^{-1}$ . Panels represent seasonal means: DJF (December–January–February), MAM (March–April–May), JJA (June–July–August), and SON (September–October–November).

selected sectors with a longitudinal angular extent  $\Delta\lambda_R$ <sup>43,63–65</sup>

$$\Psi_R(\phi, p) = \frac{\Delta\lambda_R R_e \cos \phi}{g} \int_0^p v_R(\phi, p') dp'. \quad (3)$$

Figure 1B–D shows the resulting regional MSFs for the Europe-Africa, Asia-Pacific, and Americas sectors.

This review considers the HC, focusing on aspects that are relevant for understanding the effects of climate change on its characteristics. It does not attempt to review the full body of existing knowledge on the HC, which would not be feasible within a single article. The section “Dynamics of the HC” describes the theoretical understanding of the HC dynamics (e.g., Refs. 67–71), strength and width (see the sec-

tion “Scaling of the Hadley cell”), transient behavior and its connection to monsoons (see the section “The response of the seasonal migration of the ITCZ”). The section “Links of the HC with the energy budget” describes the energy budget of the HC, how it relates to the cross equatorial energy transport and top-of-atmosphere fluxes. The section “The responses of the HC to natural and anthropogenic forcings” describes the HC response to different forcings: GHGs, stratospheric and tropospheric ozone, black carbon (BC), dust and volcanic eruptions, and astronomical cycles. The section “Regionality of the HC” describes how the regional HCs respond to climate change. The status of the knowledge, gaps, and present research needs are discussed in the “Discussion and conclusions” section.

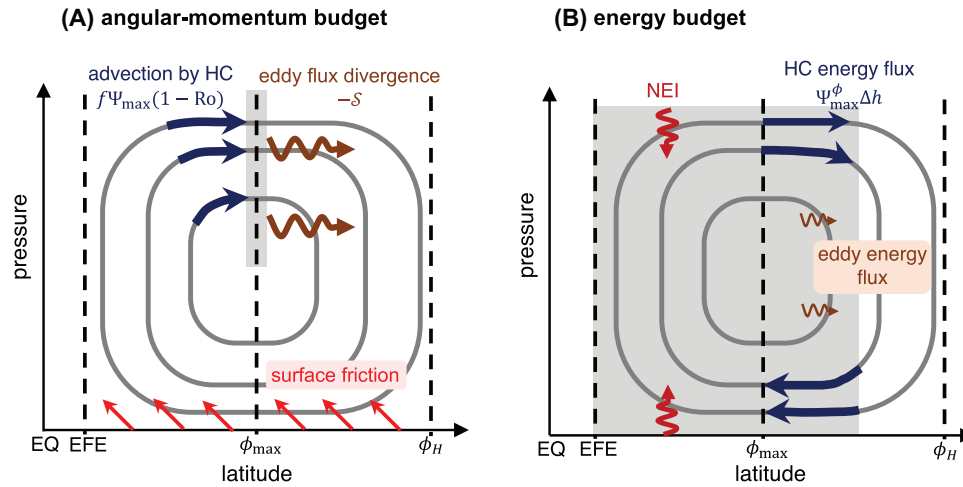


**FIGURE 3** (A) Momentum- and (B) energy-budget constraints on the HC strength. Gray lines represent streamlines of the HC and light gray boxes represent the region over which the budget is evaluated. (A) Angular momentum advection by the mean flow (blue arrows) and eddy angular momentum flux (brown arrows) as considered in Equation (4). (B) Meridional energy flux by the HC (blue arrows), eddy energy flux out of the tropics (brown arrows), and net energy input (NEI) to the tropical atmosphere (red arrows) as considered in Equations (7) and (8). EFE denotes the Energy Flux Equator, that is, the location where the atmospheric energy transport goes to zero and approximate location of the ITCZ.

## DYNAMICS OF THE HC

### Scaling of the Hadley cell

A useful starting point for understanding the dynamics of the HC is the subtropical angular-momentum budget, which expresses a balance between the advection of angular momentum into the subtropics by the mean circulation and the flux of angular momentum out of the subtropics owing to eddies (Figure 3). An approximate diagnostic for the HC strength may be derived by evaluating this budget for the upper branch at the latitude of the center of the HC (e.g., Refs. 68, 72),

$$\Psi_{\text{MAX}}(1 - \text{Ro}) \approx \frac{S}{f}. \quad (4)$$

Here, the strength of the HC is measured by the MSF maximum  $\Psi_{\text{MAX}}$ , and  $\text{Ro}$  is the Rossby number of the flow, which may be expressed approximately as  $\text{Ro} \approx -\bar{\zeta}/f$ , with  $\bar{\zeta}$  being the zonal mean vorticity evaluated in the upper-branch of the HC and  $f$  the Coriolis parameter. The numerator on the right-hand side  $S$  represents net result of the poleward transport of angular momentum provided by eddies integrated vertically between the level of the MSF maximum and the tropopause, and it represents the influence of transient and zonally asymmetric motions on the HC. Theories of the HC often consider one of two limits: in the axisymmetric limit (see the section “Axisymmetric theory”), eddy-momentum fluxes are small and  $\text{Ro} \approx 1$ ,<sup>67,73–77</sup> in the small-Ro limit (see the section “Small Rossby number theory”), the zonal mean vorticity is small compared to  $f$ , and eddy-momentum fluxes are dominant (e.g., Refs. 68, 78).

The edge of the HC is usually defined by the latitude of the zero of the MSF at a mid-tropospheric level (e.g., 500 hPa, Ref. 79). In the axisymmetric limit, this latitude is determined not by the angular

momentum balance but by the energy budget, under the requirement that the temperature at the cell edge is equal to its corresponding value in the “radiative-convective equilibrium” state in the absence of large-scale circulations.<sup>67,80</sup> In the small-Ro limit, the angular-momentum budget requires that this latitude coincides with a switch from eddy angular momentum flux divergence to convergence, and the HC edge may be identified as the equatorward margin of wave-activity generation by baroclinic eddies.<sup>81</sup> In this limit, eddies play a central role in determining both the width, as well as the strength, of the HC.<sup>68,81,82</sup>

### Axisymmetric theory

In the axisymmetric case, the atmospheric flow is assumed to have no zonal variations, the right-hand side of Equation (4) is zero, and the existence of the HC (i.e.,  $\Psi_{\text{MAX}} \neq 0$ ) requires  $\text{Ro} = 1$ . In this case, Equation (4) becomes degenerate and gives no information about the HC. Nevertheless, the requirement that  $\text{Ro} = 1$  is equivalent to requiring that angular momentum is conserved along streamlines of the flow, and it provides a strong constraint on the zonal wind distribution.

Building on the work of Schneider<sup>73</sup>, Held and Hou<sup>67</sup> derived a simple model for the equinoctial HC in the axisymmetric limit (hereafter H&H model), which was extended to the case of off-equatorial thermal forcing by Lindzen and Hou.<sup>80</sup> The theory relates the angular momentum conserving wind distribution, through the assumption of thermal wind balance and weak surface winds, to the meridional gradient of temperature. Combining this with a simple closure for the energy transport by the cell, a complete description of the HC is obtained. The H&H model predicts a finite width for the HC that, for Earth-like parameters, is comparable to the observed HC width. Moreover, the model provides scalings for the width  $\phi_H$  and strength  $\Psi_{\text{MAX}}$  of the HC

given by

$$\phi_H \sim \left( \frac{gH\Delta_h}{\Omega^2 R_e^2} \right)^{1/2}, \quad (5)$$

$$\Psi_{\text{MAX}} \sim \frac{1}{\tau} \frac{g^{3/2} (H\Delta_h)^{5/2}}{\Omega^3 R_e^2 \Delta_v}. \quad (6)$$

Here,  $\Omega$  is the Earth's rotation rate and  $\tau$  is a radiative relaxation timescale. Equations (5) and (6) involve parameters that depend on the climate conditions: the troposphere depth  $H$ , the fractional surface-to-tropopause potential temperature  $\Delta_v$ , and a measure of the fractional pole-to-equator potential temperature difference in the "radiative-convective equilibrium" solution that would exist in the absence of a circulation,  $\Delta_h$ . The H&H model (Equations 5 and 6) predicts that the strength and width of the solstitial HC increase with increasing tropospheric depth and radiative-convective equilibrium meridional potential temperature gradient, while the strength of the cell decreases with increasing thermal stratification.

### Small Rossby number theory

In the small-Ro number limit of Equation (4), the strength of the Hadley cell is directly related to the eddy angular momentum flux and its divergence in the subtropics. This flux divergence occurs primarily as a result of extratropical baroclinic eddies that form in the mid-latitudes and propagate into the subtropics, where they reach their critical latitude and break, decelerating the mean flow (e.g., Ref. 83). In the small-Ro limit, the HC does not respond directly to the thermal driving, rather, its variations are linked to those of the eddy angular momentum flux divergence in the subtropics.<sup>68,72</sup>

Theories highlighting the effect of eddies on the HC go back to the 1950s when Kuo<sup>84</sup> and Eliassen<sup>85</sup> developed a diagnostic equation connecting the meridional overturning to sources of momentum and heat associated with eddy motions and diabatic effects. A number of authors have also investigated how eddies influence the equinoctial HC by comparing the results of axisymmetric and eddy-permitting simulations of the HC using idealized models.<sup>86-91</sup> Such comparisons generally reveal that eddies substantially amplify the strength of the equinoctial HC compared to the axisymmetric case, because eddies allow the descending branch to more efficiently lose its angular momentum while approaching the boundary layer. According to Equation (4), this increases the strength of the HC. However, this amplification is much weaker if the surface temperature is specified instead of being computed by closing the surface energy balance.<sup>89,92</sup> The strength of the HC has also been found to scale with the magnitude of the divergence of the angular eddy momentum fluxes propagating into the subtropics from the mid-latitudes in a suite of simulations with an idealized GCM over a wide range of parameters.<sup>68</sup>

Concerning the width of the HC, it has been suggested that the HC terminates at the location where the axisymmetric solution would

become baroclinically unstable.<sup>82</sup> This argument has been supported by both idealized<sup>81</sup> and comprehensive<sup>44</sup> climate change modeling studies, as well as by reanalysis studies of interannual variability,<sup>93</sup> which reveal strong relationships between diagnostics associated with extratropical eddies and the width of the HC (e.g., Refs. 94-97). Moreover, it is consistent with the observed narrowing of the HC in response to El-Niño,<sup>98,99</sup> which is associated with increased meridional temperature gradients in the subtropics and an equatorward displacement of the storm track.

### The seasonality of the HC and its response to climate change

Earth's tropical overturning circulation undergoes an annual cycle where the equinoctial HC, characterized by two cells of roughly equal strength and the ITCZ close to the equator, represents a transitional condition between two solstitial states, each characterized by a strong cross-equatorial HC cell (which has its descending/ascending branch in the winter/summer hemisphere) and a weaker cell in the summer hemisphere.<sup>50</sup> The poleward flow of both equinoctial HC cells and the whole solstitial summer cell occur in regions of upper-tropospheric westerlies, through which mid-latitude eddies are able to propagate. These cells are, therefore, strongly influenced by eddy transports of energy and momentum<sup>68</sup> and are close to the small-Ro regime (see the section "Small Rossby number theory"). At the solstices, however, the existence of easterlies in the equatorial upper troposphere prevents Rossby waves from propagating into the deep tropics, limiting the influence of eddies on the HC upper branch,<sup>72,100,101</sup> and suggesting that axisymmetric dynamics (see the section "Axisymmetric theory") is more relevant for the cross-equatorial solstitial HC. However, eddies still have important effects on the solstitial HC through their effect on the descending branch.<sup>102,103</sup>

### The response of the HC width

Motivated by both the axisymmetric theory of H&H and theories based on the onset of baroclinic instability,<sup>82</sup> a number of studies have investigated how changes in bulk thermodynamic characteristics of the troposphere under climate change affect the HC width (e.g., Refs. 104, 105). Under global warming, the tropopause height and stability are expected to increase,<sup>106</sup> while the meridional temperature gradient in the subtropical atmosphere decreases.<sup>104,107</sup> Analysis of different climate conditions using PMIP simulations and RCP8.5 projections indicate that, under solstitial conditions, the HC widens as the subtropical static stability and the tropospheric depth increase, while its dependence on meridional temperature gradient differs between the hemispheres.<sup>105</sup> This leads to the relatively robust result that the HC becomes wider as the climate warms.<sup>105,108</sup>

While the above results are qualitatively consistent with the H&H scalings embodied in Equations (5) and (6), this should not be taken as a conclusive argument supporting them as all involved variables

are correlated among themselves and very well correlated with global warming.<sup>105</sup> In fact, a growing literature suggests that both in equinoctial and solstitial conditions, the HC width is strongly influenced by midlatitude processes,<sup>81</sup> scaling with the equatorward-most location at which the mean state is baroclinically unstable.<sup>82</sup> For example, Chemke and Polvani<sup>109</sup> analyzed the detailed time evolution of the HC under abrupt 4xCO<sub>2</sub> forcing to show that variations in the subtropical baroclinicity give the best explanation for the simulated shifts in the HC edge. According to this interpretation (e.g., Refs. 28, 44, 110), the projected widening of the HC is associated with increased static stability, reduced meridional temperature gradients in the subtropics, and a poleward shift of the storm track (e.g., Ref. 27) as seen under La-Niña condition.<sup>99</sup> However, directly relating these changes in the HC width to the influence of eddies or any other external factor remains challenging.<sup>107</sup> Diagnostic relationships between eddy-forcing and shifts in the HC should be cautiously used as an evidence of causality, and the widening of the HC under warming has instead been argued to be an axisymmetric response, with eddies acting as a damping factor to reduce its magnitude.<sup>111</sup>

### The response of the HC strength

For the strength of the HC, both axisymmetric and small-Ro dynamics may be important, and the relative importance depends on the point in the seasonal cycle being considered. The axisymmetric theory suggests that the HC strengthens with increasing tropospheric depth and meridional temperature gradient, but it weakens with increasing thermal stratification. These scalings, based on the H&H model, have been investigated under different climate conditions using PMIP simulations and RCP8.5 projections<sup>105</sup> showing that the Northern Hemisphere (NH) solstitial HC strength scales with the tropospheric depth, the fractional pole-to-equator potential temperature difference  $\Delta h$ , and the subtropical near-surface static stability, while a weak and unclear dependence is present for the SH. However, the complex superposition of different responses limits the potential for theoretical constraints on the changes in the HC strength that are produced under future warming scenarios; for example, Chemke and Polvani<sup>112</sup> point out the importance of the direct effect of CO<sub>2</sub> forcing, independent of surface temperature changes. Complicating matters further, idealized simulations suggest that the change in equinoctial HC strength with warming may be nonmonotonic, with changes in eddy fluxes, Rossby number, and ocean heat transport all playing a role.<sup>113</sup>

### The response of the seasonal migration of the ITCZ

At the solstices, the winter cell dominates the tropical overturning circulation, shifting the zonal mean precipitation maximum into the summer hemisphere and transporting energy across the equator to the winter hemisphere (see the section “Links of the HC with the energy budget”). At the same time, monsoon circulations develop over tropical continents, with associated precipitation providing water for over

half the world's population (e.g., Ref. 114). While, historically, monsoon circulations have often been conceptualized as large-scale land-sea breezes, with the land-sea contrast considered to be central to their behavior, more recent studies show that monsoons are the regional expression of the seasonal migration of the ITCZ at the solstices (see, e.g., Refs. 100, 115). In this view, individual regional monsoons are components of the global monsoon system, and changes in the HC and the global monsoon system are fundamentally coupled (e.g., Ref. 116). Such a view does not preclude a role for land-sea contrasts in influencing the local behavior of individual monsoons.<sup>117</sup>

The axisymmetric theory shows that a shift of the thermal forcing maximum by a few degrees from the equator<sup>80</sup> or an isolated, off-equatorial thermal maximum above a low threshold<sup>118</sup> are sufficient to trigger the transition to the regime dominated by a single (winter) HC. Realistic time-dependent cases<sup>76,88</sup> and observed estimates of the zonal mean circulation<sup>50</sup> show that this transition is less pronounced than in the idealized theoretical description. Further, feedbacks associated with stationary eddies<sup>119,120</sup> and surface fluxes<sup>121</sup> have a potential role in accelerating the transition between regimes, while surface flux feedbacks and cloud-radiative interactions have a role in the timing and in increasing the rapidity of the onset of the Asian monsoon.<sup>122</sup> A number of recent studies have investigated the sensitivity of the seasonal migration of the ITCZ to the planetary rotation rate.<sup>69,70,123-125</sup> Under climate change, Seth et al.<sup>126</sup> found a delay in the onset of a number of monsoons, attributing this to an increased convective springtime barrier in a warmer world (similar to the so-called upped-ante mechanism.<sup>127</sup>) However, detailed understanding of how climate change affects the dynamics of the HC seasonal cycle remains a work in progress.<sup>116</sup>

## LINKS OF THE HC WITH THE ENERGY BUDGET

The energy budget couples the HC to the net input of energy into the tropical atmosphere by radiative and turbulent fluxes on the one hand, and eddies on the other hand, providing a complementary constraint on the HC strength to the momentum-budget-based constraint embodied in Equation (4) (see Figure 3). In this section, energetic arguments are used to provide a framework to understand the HC response to global warming. Indeed, the primary effect of GHG emissions is to perturb the energy balance at the top-of-atmosphere (TOA), while the thermodynamics and circulation responses work toward re-establishing the energy balance.

### Meridional energy transport by the HC

Air masses diverging from the ITCZ are drier and cooler than those converging at low level, but they also have significantly higher potential energy. As the latter effect dominates (Figure 4), the moist static energy (MSE, in J/kg,  $m = C_p T + gZ + L_v q$ , where  $C_p$ ,  $T$ ,  $g$ ,  $Z$ ,  $L_v$ , and  $q$  are heat capacity, temperature, gravity, geopotential height, latent heat of vaporization, and specific humidity, respectively) of air masses aloft is

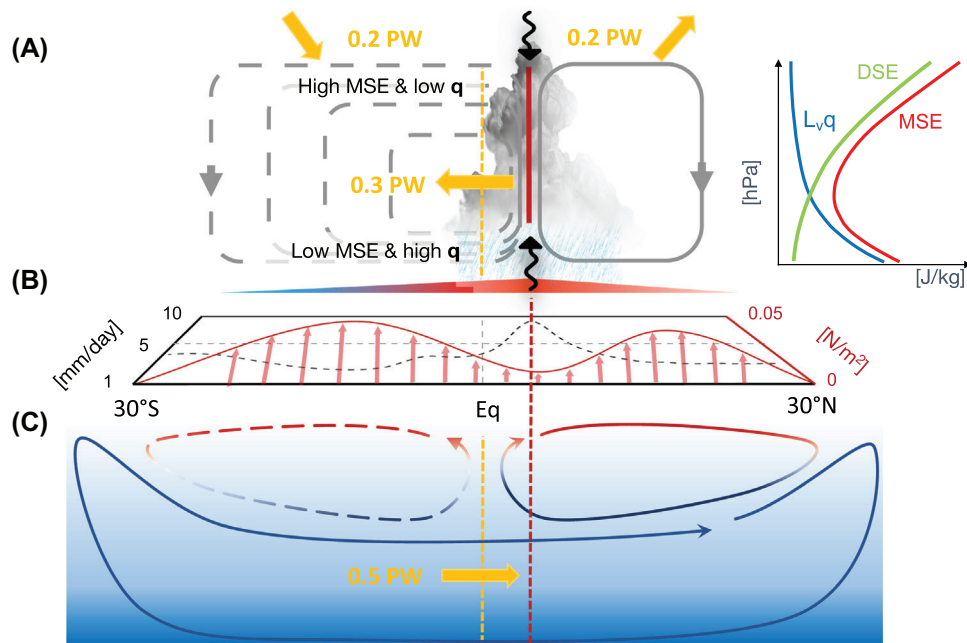


**FIGURE 4** Schematic of the Hadley circulation and associated energy transport. (A) Annual mean Hadley cell (gray) and typical vertical profiles of moist static energy, dry static energy, and latent heat. (B) Schematic meridional profile of precipitation (dashed black line) and surface wind stress (solid red line with arrows). (C) Overturning circulation in the ocean showing the subtropical cells and the Atlantic overturning circulation.

higher than of those at low levels. The net effect is that, in the vertical integral, the HC exports energy away from the ITCZ while simultaneously importing moisture into the ITCZ. This net meridional energy transport, often described as the atmospheric heat transport  $AHT$ , scales as Refs. 128, 129:

$$AHT(\phi) \simeq \Psi_m(\phi) \cdot \Delta \bar{m}(\phi) + T_e(\phi), \quad (7)$$

where  $\phi$  is the latitude,  $\Delta$  denotes the difference between upper and lower branches of the HC, the overbar denotes the zonal mean,  $\Psi_m$  is the maximum of the global MSF as a function of latitude (kg/s), and  $T_e$  is the eddy meridional heat transport (vertically and zonally integrated). The  $AHT$  is dominated by the overturning term in the Tropics<sup>130</sup> where horizontal gradients, and thus  $T_e$  are small (see Figure 3).  $T_e$ , however, becomes dominant away from the Equator. The total  $AHT$  can be decomposed into dry static energy ( $DSE = C_p T + gZ$ ) and latent heat ( $LH = L_v q$ ) transport, which can be obtained (again at the scaling level) as  $AHT_{DSE} \simeq \Psi_m \cdot \Delta \bar{DSE}$  and  $AHT_{latent} \simeq \Psi_m \cdot \Delta \bar{LH}$ , respectively. Since  $LH$ , which depends on the humidity  $q$ , decreases with height, while the  $DSE$  increases with height (Figure 4),  $AHT_{DSE}$  and  $AHT_{latent}$  oppose one another. Using typical values for Earth's atmosphere,  $\Psi_m \simeq 100 \times 10^9$  kg/s and  $\Delta \bar{m} \simeq 10^4$  J/kg, Equation (7) gives about 1 PW, typical of the  $AHT$  near the peak of the HC MSF.<sup>130–132</sup> Observations<sup>133</sup> reveal a robust linear relationship between  $\Psi_m(0)$  and  $AHT(0)$  through the seasonal cycle, consistent with a constant value of  $\Delta \bar{m} \simeq 1.4 \times 10^4$  J/kg, emphasizing that, close to the equator, the time (seasonal) variations in  $AHT$  are dominated by changes in the strength of the HC.

$AHT$  is related to the Net Energy Input ( $NEI$ ) in the tropical troposphere, which is given by the vertical integral of the diabatic heating

(see Figure 3) or, equally, the difference between the net radiative fluxes at the top of the atmosphere and net radiative and turbulent fluxes at the surface. In fact, at steady state, the vertically and zonally integrated energy budget of the tropical atmosphere is a balance between the rate at which energy is transported away from the ITCZ (given by the meridional divergence of  $AHT$ ) and the zonally averaged (positive)  $NEI$ :

$$\frac{\partial AHT}{R_e \partial \phi} = 2\pi R_e \cos(\phi) \cdot \overline{NEI}. \quad (8)$$

Using a two-layer description of the atmosphere,<sup>134</sup> connected the  $NEI$  to the vertical motion and energy stratification showing that:

$$NEI \simeq -\frac{\omega_m}{g} \cdot GMS, \quad (9)$$

where  $\omega_m$  (Pa/s) is the vertical velocity at a mid-tropospheric level  $p_m$  separating the upper and lower part of the troposphere. The Gross Moist Stability ( $GMS$ , J/kg) is the difference between the horizontal flow divergence-weighted averaged MSE of the upper and lower layers and it can be considered a representation of the transport of MSE away from the tropics by the divergence of the mean circulation. In fact, Equation (9) is a valid approximation only under the assumption that the advection of MSE by the mean circulation and its transport by eddies are negligible. Physically, Equation (9) states that, in the deep tropics, where horizontal gradients are weak, ascent ( $\omega < 0$ , a conversion of air parcels from low to high MSE) requires a diabatic energy source ( $NEI > 0$ ; see Figure 3, right panel). However, since the flow is strongly divergent,  $NEI$  can be only partially converted in the MSE of the

upper troposphere, and the concept of *GMS* is needed for expressing the relation between *NEI* and convection. Equation (9) loses its relevance away from the equator such that, in the descending branch, the decrease of potential energy and adiabatic warming are balanced by a poleward energy export by eddies (Figure 3).

The *GMS* concept has been extensively used in the subsequent literature and often been redefined.<sup>134–138</sup> Although all its definitions measure the vertical variations of *MSE*, *GMS* has also been interpreted as an efficiency of the meridional heat transport by the HC or a measure of the energy export per unit convective mass flux.<sup>139,140</sup> Both  $\Delta m$  and *GMS* are nearly always positive in the tropical atmosphere,<sup>135</sup> because energy is larger in the upper than in the lower tropical atmosphere, though negative *GMS* can occur depending on the choice of definition and inclusion, or not, of advection and transient terms (neglected in Equation 9).

Equation (9) implies a tight link between changes in *GMS* (or  $\Delta m$ ) and changes in vertical velocity:

$$\frac{d\omega_m}{\omega_m} = -\left(\frac{dGMS}{GMS} + \frac{dNEI}{NEI}\right) \simeq -\frac{dGMS}{GMS}, \quad (10)$$

where the second equality is obtained in the limit of small *NEI* changes. Equation (10) provides the link between the strengthening of the stratification and weakening of the overall tropical circulation including the HC. Global warming, on one hand, increases the water vapor concentration in the lower troposphere, therefore, reducing *GMS*, on the other hand, warms the upper troposphere and uplifts the tropopause, therefore, increasing *GMS*. The increase prevails so that  $\omega_m$  and the overall tropical circulations weaken (see Refs. 137, 141 and references therein). The increase of *GMS* and weakening of the circulation, respectively, increases and decreases the energy export out of the tropics (Equation 7). The two effects roughly cancel out, consistently with the assumption of relatively small *NEI* changes in Equation (10). However, *NEI* increases with GHG emissions leading to a small intensification of *AHT* (about 0.25 PW at the peak *AHT* in both hemispheres [see Ref. 142]).

## The ITCZ latitude and cross-equatorial energy transport

Because both vertical *MSE* gradient and *MSF* are weak at the ITCZ, *AHT* is small and changes sign near the ITCZ. In practice, the “energy flux equator” (EFE, where *AHT* = 0, Figure 3) is close to the ITCZ, although they are not always collocated,<sup>133,143</sup> because of small, but non-negligible, eddy fluxes in Equation (7). In the present-day climate, the ITCZ is located on average about 5° N and this meridional deviation is most pronounced in the Pacific Ocean (see, e.g., Ref. 143). As the distribution of incoming solar radiation is nearly symmetric around the equator, it was suggested this asymmetry was due to land mass distribution and/or ocean–atmosphere coupling.<sup>144</sup> As detailed below, recent studies, using an energy perspective, suggest that the latter effect is the dominant one.

The latitude of the zero energy transport,  $\delta$ , is obtained by a Taylor expansion<sup>143</sup>:

$$AHT(\delta) \simeq AHT(0) + \frac{\partial AHT}{\partial \phi}(0) \cdot \delta = 0, \quad (11)$$

which, using Equation (8), gives:

$$\delta = -\frac{1}{2\pi R_e^2} \cdot \frac{AHT(0)}{\overline{NEI}(0)}. \quad (12)$$

Using  $\overline{NEI}(0) = 18 \text{ W m}^{-2}$ , and *AHT*(0) = –0.3 PW,<sup>143,145</sup> one obtains  $\delta \sim 4$  degree of latitude, which is in close agreement with observations. Equation (12) highlights that the off-equator location of the ITCZ depends on the ratio between the energy transport at the equator (dominated by the HC) and the net energy input. It suggests that a larger  $\overline{NEI}(0)$  would shift the ITCZ closer to the equator at constant *AHT*(0). However, under climate change, both  $\overline{NEI}(0)$  and *AHT*(0) are expected to change. Indeed, in 2xCO<sub>2</sub> experiments with slab ocean from CMIP3 (Coupled Model Intercomparison Project 3),<sup>146</sup> found northward/southward ITCZ shifts which are well correlated with decreased/increased *AHT*(0). This is consistent with Equation (12) although suggesting that *AHT*(0) changes dominate over the  $\overline{NEI}(0)$  changes in these experiments.

## Linking the ITCZ position with ocean heat transport, TOA flux, and SST

The SH receives about 0.4 PW more than the NH, as the TOA, hemispheric *NEI* is positive for the SH (+0.2 PW) and negative for the NH (–0.2 PW).<sup>147,148</sup> This asymmetry is dominated by the outgoing long-wave radiation, presumably because the NH is slightly warmer than the SH.<sup>149</sup> The short-wave difference between the two hemispheres is small as they have similar average incoming solar radiation and similar planetary albedo ( $\sim 0.3$ , see Ref. 133). Current best estimates suggest a global ocean heat transport (OHT) of about 0.5 PW northward across the equator,<sup>150,151</sup> which is mostly achieved in the Atlantic basin with a transport of  $\sim 0.7$  PW, while the Pacific Ocean is close to neutral and the Indian Ocean transports  $\sim 0.2$  PW southward (all these estimates have the significant uncertainties of about  $\pm 0.2$  PW). The large Atlantic transport is primarily driven by the Atlantic Meridional Overturning Circulation (AMOC) associated with deep water formation in the Nordic seas and Labrador sea.<sup>152</sup> In the absence of deep water formation in the Pacific and Indian oceans, their transports are dominated by shallow wind-driven subtropical overturning cells (STCs). The global northward OHT combined with the 0.3 PW southward transport by the HC balances the TOA radiation asymmetry and closes the energy budget of both hemispheres (Figure 4).

The hemispheric energy balance suggests that the northward position of the ITCZ compensates for the northward cross-equatorial OHT.<sup>147,153</sup> This agrees with atmospheric model experiments in which the OHT is prescribed (so-called Q-flux experiments, see Refs. 143 and 154 and references therein), where the ITCZ moves

northward/southward as the (implied) cross-equatorial OHT is increased/decreased. The ITCZ shift is not seen only in the AMOC-dominated Atlantic sector, but also in the Pacific because of the efficiency of the atmosphere to zonally redistribute the energy output.<sup>155</sup> Variations of the AMOC strength in past and future climates are, therefore, expected to contribute to the displacement of the ITCZ compared to present-day (intensification of AMOC would move the ITCZ northwards and further away from the Equator [see below Ref. 47]).

The mechanisms re-establishing the energy balance and connecting the ITCZ to the OHT variations are likely provided by the interhemispheric sea surface temperature (SST) difference across the equator that is caused by the AMOC OHT warming the NH and cooling of the SH. A robust linear relationship between ITCZ shifts and changes in interhemispheric tropical SST difference ( $20^{\circ}\text{N} - 0$  minus  $20^{\circ}\text{S} - 0$ , in K) can be found in observations and climate models (with slopes of 3.3 and 3.7 K/deg of latitude, respectively<sup>133</sup>) and under other climates (although with weaker slopes in the range 1.5–2.4 K/deg for last glacial maximum, mid-Holocene, and  $2\times\text{CO}_2$ ). Such relationships combined with paleo-proxy estimates of temperature can be used to reconstruct the global ITCZ shifts.<sup>47</sup> Numerical experiments with an imposed cross-equatorial flux demonstrate that the ITCZ is sensitive to high latitude SST perturbations (e.g., Ref. 156), possibly generated by AMOC changes (see example in Ref. 157) and explained by a “rigidity” imparted to the AHT by the weak temperature gradient in the tropics.<sup>143</sup> In climate model projections, the AHT anomaly is directed from the faster to the slower warming hemisphere.<sup>149</sup>

The STCs and HC are coupled through the wind stress at the air-sea interface (Ref. 128, Figure 4). If the effect of eddy momentum fluxes in the atmospheric boundary layer is neglected, the STC and HC should have opposite mass transports of similar magnitude. However, the STCs are more efficient at exporting heat away from the equator than the HC because the temperature stratification in the ocean is stronger than in the atmosphere.<sup>129</sup> The result is that the coupling between the ITCZ shift and the response of the STCs generates a negative feedback that can limit the excursions of the ITCZ in response to perturbations.<sup>158</sup>

## THE RESPONSES OF THE HC TO NATURAL AND ANTHROPOGENIC FORCINGS

### HC trends in the last decades

For a long time, behaviors of the HC and interpretation of long-term trends in reanalyses were considered uncertain due to the influence of natural variability, which in the late 19th and early 20th century may have exceeded the changes that occurred in the recent decades,<sup>159</sup> and due to different model physics and data assimilation methods adopted by reanalyses.<sup>40, 98, 160</sup> In spite of that, there is general agreement among reanalyses that the global HC has significantly widened in the last four decades, while changes of the HC strength are still uncertain and data-dependent.<sup>31, 32, 98, 110, 159–162</sup>

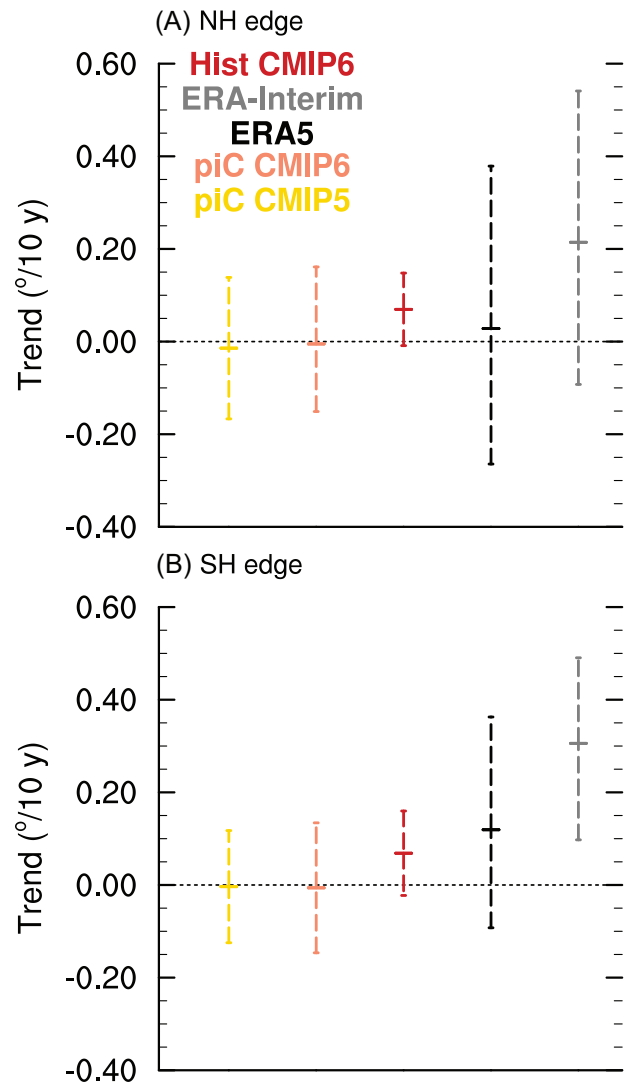


**FIGURE 5** Annual trends of the HC edges in the period 1979–2014: for ERA5 (black), ERA-Interim (gray), the central line marks the Sen's estimate and whiskers the 95% confidence interval; for the All-forcing historical simulations (red), the CMIP6 (orange), and CMIP5 (yellow) PIcontrol (piC) the central line marks the multimodel mean value and whiskers indicate the range of possible trends (i.e., twice the intermodel standard deviation,  $2\sigma$ ). Positive/negative trends indicate poleward expansion/contraction of the HC. Units are latitude degrees per decade for the edges (based on Refs. 164 and 165).

Figure 5 compares the HC extension trends in the ERA5<sup>66</sup> and ERAInterim<sup>163</sup> reanalyses, to those of the CMIP5 and CMIP6 historical “All-forcing” (based on Ref. 164) and preindustrial control (PIcontrol) experiments (based on Ref. 165). The period 1979–2014 is used to avoid the comparison between model simulations and reanalysis before the large increase of satellite data starting in 1979. Though the reanalyses contain structural problems and systematic errors,<sup>160–162</sup> there are indications that these issues do not prevent a realistic reconstruction of the past HC evolution. Figure 5 shows that the HC expansion in reanalyses (particularly in ERA5) is within the range of models’ “All-forcing” experiments,<sup>165–168</sup> with former reanalyses (such

**TABLE 1** Summary table of the impact of various forcings on the HC strength and width.

Factor	Past decades	Projections
GHG	Widening and weakening	Widening and weakening
Stratospheric O <sub>3</sub>	Widening (stronger in the SH)	Narrowing (stratospheric O <sub>3</sub> recovery)
Anthropogenic aerosols	ITCZ southward shift, uncertain and minor contraction, NH strengthening	Depending on aerosol emission
Tropospheric O <sub>3</sub>	NH widening (uncertain)	
Volcanism	Temporary (1–3 years) ITCZ narrowing, uncertain effect on HC width	
All	Widening, uncertain effect on strength, large role of natural variability	Widening (larger in the SH) and weakening (larger in the NH)
Glacials	Strengthening and narrowing of solstitial circulation	Strengthening and narrowing of solstitial circulation

as ERAInterim) being just compatible with the largest “All-forcing” trends.<sup>107, 110, 160, 165, 169</sup> This comparison suggests that internal variability has a large impact on long-term trends and that structural problems (in climate models and reanalyses) may limit our ability to assess HC trends convincingly.<sup>160</sup> However, by accounting for internal variability and different HC metrics, climate model and reanalysis results can be reconciled.<sup>32, 165, 166, 170</sup> AMIP simulations show that the value of the trends of HC width since the last two decades of the 20th century have been affected by the variability of SST patterns via coupled atmosphere–ocean dynamics.<sup>107, 167, 171, 172</sup> Modes of variability like El Niño–Southern Oscillation (ENSO) and Pacific Decadal Oscillation (PDO), particularly the change in the phase of the PDO from positive to negative during the late 1990s approximately doubled the rate of tropical expansion from that expected from anthropogenic forcing alone.<sup>107, 167, 171</sup> In fact, Figure 5 shows that trends of magnitude comparable to those in the reanalyses are present in the Plcontrol simulations as a result of the internal variability alone.

Trends of HC strength and width are caused by the superposition of multiple factors due to internal variability, natural and anthropogenic forcings (e.g., GHGs, stratospheric and tropospheric ozone, aerosols, particularly BC, volcanic eruptions, and orbital forcing). Disentangling the individual impacts of natural and anthropogenic forcings on the recent HC evolution is possible by designing single-forcing experiments in an ensemble context. The following subsections discuss the response of HC strength and width to different forcings, highlighting the structural difficulties and consequent uncertainties in CMIP sensitivity experiments in Figure 6, where, as in Figure 5, we have considered the period 1979–2014 instead of 1970–2014 originally used in Ref. 164.

The analysis of the impact of various forcings on the HC strength and width that is provided in the next subsections is largely guided by the CMIP experiment prescriptions, that is, GHG, stratospheric ozone (StratO3), anthropogenic aerosols (Aer), and natural forcings (Nat) as shown in Figure 6, but it also considers literature on the role of BC, tropospheric ozone, and the HC response to orbital forcings. Table 1 provides a synthesis of the impacts of the considered factors. Results based on dedicated CMIP simulations suggest widening and narrow-

ing of the HC, as a consequence of GHG and anthropogenic aerosols increasing, respectively. In Figure 6 (updated from Ref. 164), these contrasting effects are pronounced on the SH HC, and not evident in the NH HC. However, the simulations of Figure 6 may be not fully adequate for describing the role of some factors, such as BC and some species of anthropogenic aerosols that have a negligible effect on the global HC, but may be important at regional scale (see the section “Past and projected changes of the regional HCs under anthropogenic climate change”). Further, the different number of models that were available for the experiments in Figure 6 (27 for All-forcing, 10 for GHG, 3 for Stratospheric ozone, 9 for Aerosols, and 11 for Natural forcing) may affect the relative magnitude of the changes among different experiments, which may not be a function only of the forcings. Moreover, in Figure 6, individual single forcing trends should not be expected to add up to the “All-forcing” scenario trends, because different subsets of models have been used for each experiment.

For the sake of clarity, we restrict the literature review to the aforementioned forcings, although stratospheric aerosol geo-engineering,<sup>173</sup> water vapor<sup>174</sup> and Arctic sea ice loss<sup>175</sup>, wildfires,<sup>176</sup> and natural dust emissions<sup>177</sup> have been proposed to significantly shape the HC too.

## CO<sub>2</sub> and other well-mixed GHG

The large majority of climate model simulations show that weakening of the HC is the prevalent effect of the GHG-induced global warming. In fact, the weakening of the solstitial winter HC is significant in CMIP5 and CMIP6’s GHG simulations for the period 1979–2014. There is also consensus on the weakening<sup>44, 105, 137, 178</sup> in climate projections, though with a large uncertainty on its magnitude, ranging between 0% and 4% K<sup>-1</sup> as a function of the global-mean surface air temperature change.<sup>44, 105</sup> The weakening of the HC is qualitatively consistent with the decrease in ascent and associated increase in GMS, as predicted by the simplified energy balance Equation (10) (see the section “Meridional energy transport by the HC” and Ref. 137). Dynamical theories of the HC do not provide a clear interpretation of the

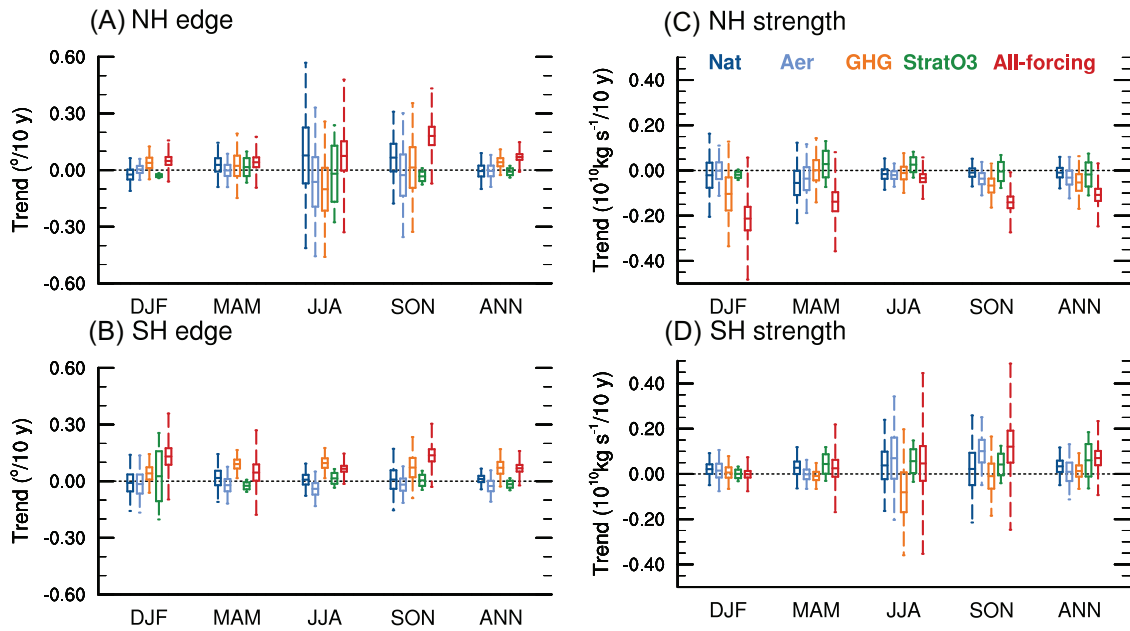


**FIGURE 6** Trends of the HC edges (left) and strength (right) in the period 1979–2014 for ERA5 (black), ERA-Interim (gray), and CMIP6 historical simulations: All-forcing (red), GHG (orange), Stratospheric ozone (StratO3, green), Aerosols (Aer, light blue), and Natural forcing (Nat, blue). Positive trends indicate poleward expansion/strengthening and negative trends contraction/weakening of the HC. Units are latitude degrees per decade for the edges and  $\text{kg/s}$  per decade for the strength. In color whisker-box (CMIP6), the central line marks the multimodel mean value of the trends. Boxes indicate uncertainties on the multimodel mean trends (i.e., twice the standard error,  $2\sigma/\sqrt{n}$ , where  $\sigma$  is the standard deviation of the trends and  $n$  is the number of CMIP6 models that have been analyzed in each set of simulations), while whiskers indicate the range of possible trends (i.e., twice the standard deviation,  $2\sigma$ ). Note that the latter is a slight underestimate of the true range of possible realizations as some, but not all, model trends are obtained through ensemble averaging (adapted from Ref. 164).

effect of GHG-induced warming on the HC intensity. For instance, according to the H&H model, on one hand, the decrease of the meridional temperature gradient and the increase of vertical stratification in the tropics caused by GHG emission weaken the HC. On the other hand, the increase of the tropospheric depth strengthens the HC (see the section “Axisymmetric theory” and references therein).

Model simulations show that GHG increase leads to HC widening. In the CMIP5 and CMIP6 simulations considered in Figure 6, the HC expansion driven by GHGs is larger in the SH than in the NH, being significant in the SH in every season, in the NH at the annual scale, and in the winter solstitial season. In fact, there is a consensus that GHGs have contributed to HC widening since 1980 in idealized simulations<sup>79, 179–181</sup> and in the different generations of CMIPs<sup>31, 44, 49, 59, 105, 109, 164–166, 182, 183</sup> especially in the SH. The asymmetry among hemispheres has been highlighted in a set of idealized (quadrupled  $\text{CO}_2$ ) simulations, which explained it as a result of the smaller sensitivity of the Northern Hemisphere HC to static stability changes<sup>181</sup>. However, seasonal details of Figure 6 differ with respect to other periods in reanalyses and to climate model simulations, which fail to reproduce the large values found in reanalysis products,<sup>107, 160, 165</sup> as natural variability (see the text at the beginning of the section “HC trends in the last decades”) and other factors (see particularly the section “Stratospheric ozone”) need to be taken into account. Further, Figure 6 is not consistent with the expectation that the GHG effect on the NH HC expansion is larger in autumn (SON) than in

other seasons.<sup>181</sup> As this expectation is based on a quadrupled  $\text{CO}_2$  concentration<sup>181</sup> and the selection of a different (longer) 1970–2014 period would produce a large HC NH expansion in SON,<sup>164</sup> the magnitude of the GHG forcing and of the SST coupling has plausibly a role on this specific seasonal feature. The expansion of the HC is expected in the small-Ro limit, consistent with the northward shift of the storm track and the eddy activity changes (see the section “Small Rossby number theory”), while the H&H model provides ambiguous indications, as it suggests on one hand an expansion of the HC under GHG forcing, as tropospheric depth is expected to increase, and on the other hand, a contraction as the meridional temperature gradient is expected to decrease (see the section “Axisymmetric theory”).

As in the next decades, without successful mitigation actions, GHG forcing will become dominant, weakening (particularly in the NH<sup>112</sup>) and widening (particularly in the SH<sup>181</sup>) of the HC shown in climate projections are expected for the future.

### Stratospheric ozone

Stratospheric ozone depletion has been identified as the primary driver of most of SH tropospheric circulation changes in DJF from 1979 until late 1990s.<sup>184</sup> Its immediate effect is to cool the lower-stratospheric polar cap, where the persistent low temperatures and strong circumpolar winds, also known as the polar vortex, prevent meridional mixing

and support the formation of a large Antarctic ozone hole. Stratospheric ozone depletion drives the poleward shift of the jet-stream which is intimately related to mid-latitude eddy activity. Therefore, according to the small-Ro theory, the HC strength and width must respond to this specific forcing.<sup>185</sup> Dedicated simulations and CMIP5 and CMIP6 stratospheric ozone experiments<sup>26, 59, 164, 182, 183, 186–191</sup> simulate widening and modest strengthening of the SH HC in response to this forcing. The relationship between the HC edge and stratospheric ozone concentration found in SH is also seen in the NH in a different set dedicated of model experiments.<sup>192</sup> The SH HC trends have slowed down since the 2000s and this hiatus has been attributed to the recovery of the stratospheric ozone.<sup>183, 184, 193</sup> Therefore, Figure 6 is not optimal to show the effects of ozone depletion, because the considered period (1979–2014) includes a relatively long sub-period during which ozone recovery occurred. Further, the shown results may not be fully representative, because the number of simulations in the StratO3 experiment is very small. While until the 2000s ozone depletion has contributed to the extension of the SH HC in synergy with GHG increase, its subsequent and future recovery acts in the opposite direction and the overall future evolution of the HC will depend on the net effect of CO<sub>2</sub> and other anthropogenic emissions.<sup>183, 184, 193</sup>

### Anthropogenic aerosols, BC, and tropospheric ozone

In the 20th century, anthropogenic aerosols (sulfate, BC, organic carbon) have exerted a cooling effect, notably over the industrial areas of the NH, that has partially compensated the GHG-induced warming,<sup>194, 195</sup> leading to a global climate evolution quite different from what would have resulted from an increase in GHG concentration alone.<sup>149</sup> The cooling of the NH relative to the SH drives a decrease in the magnitude of the southward energy transport across the equator and a corresponding southward ITCZ shift (see the section “The ITCZ latitude and cross-equatorial energy transport” and Refs. 196–199) and a deceleration of both SH subpolar and subtropical jets.<sup>200</sup> Since, in contrast to GHGs, past aerosol forcing has warmed the stratosphere and cooled the upper troposphere, it has been suggested that its effect on atmospheric circulation opposes to that of GHGs.<sup>201</sup> In fact, Allen and Ajoku<sup>202</sup> have shown that in the NH the widening associated with the increase in GHGs has been partially offset by the increase of anthropogenic aerosols in the past (when comparing to the preindustrial period, i.e., since 1850), while it is expected to be reinforced during the 21st century by the aerosol decrease that will contribute to the poleward shift in the latitude of maximum baroclinicity. However, these estimates strongly depend on whether models include the aerosol indirect effect (mainly on cloud albedo and lifetime), which are subject to uncertainties, and aerosol forcings may differ from observations.<sup>202</sup> In the SH, the zonal mean circulation changes due to aerosols are not simply opposite to those due to the GHGs<sup>203</sup> and are uncertain.<sup>204</sup> Considering intensity, strengthening of the tropical circulation driven by aerosol-induced NH cooling is consistent with thermodynamic scaling arguments.<sup>205</sup> Considering the last decades of the 20th century, the

CMIP6 simulations<sup>164</sup> summarized in Figure 6 confirm former CMIP5 results<sup>183, 202</sup> that aerosol forcing has had only a minor effect on the HC width, while they show some strengthening of the SH HC that was not present in CMIP5 experiments.

Tropospheric ozone and BC, resulting from the combustion of fossil fuels and biofuels, are both very effective warming agents and have been concentrated over the NH industrial regions for several decades of the 20th century, motivating investigation of their combined effects.<sup>169</sup> While tropospheric ozone is not an aerosol itself, its effect can only be reproduced in CMIP-type simulations with an active photochemical module describing its formation where aerosols are involved.<sup>206</sup> Unfortunately, only two models satisfying this requirement are included in the CMIP aerosol experiments shown in Figure 6 and, further, they share with similar models substantial inaccuracies when compared with tropospheric aerosol observations.<sup>206</sup> Therefore, the representation of the effect of tropospheric ozone in Figure 6 is possibly poor. The combined effect of BC and tropospheric ozone induces heating of the NH lower troposphere and perturbs the tropical boundary layer moisture, a condition that affects the climate of arid/semi-arid regions.<sup>207</sup> It also contributes to the observed poleward shift of the jet-stream, thereby relocating the main division between tropical and temperate air masses.<sup>169, 208</sup> Sensitivity experiments with a model including a detailed aerosol physics suggest that increases of tropospheric ozone and BC have been the largest contributors to the recent (1979–2009) observed widening of the NH HC, having had an effect larger than that of GHG.<sup>169</sup>

### Natural forcing: Volcanic aerosols and solar irradiance

Large volcanic eruptions inject sulfur particles into the lower stratosphere, where they reflect the incoming solar radiation and absorb solar near-infrared and thermal radiation, producing an overall global cooling effect.<sup>209</sup> The temporary radiative cooling over land (from 1 up to 3 years after the eruption) suppresses clouds, weakens tropical deep convection and the rising branch of the HC, and causes a contraction of the ITCZ.<sup>210–214</sup> Effects persist for at least two summers after volcanic eruptions.<sup>214–218</sup> The contraction of the tropical belt and of the HC following major volcanic events is shown by proxy reconstructions over the last 800 years and simulations of the last millennium.<sup>215, 219–221</sup> Narrowing has been of the order of 0.4–1° in response to Pinatubo-like eruptions and stronger (up to 1.6°) for events of double this magnitude.<sup>221</sup>

In CMIP protocols, volcanic eruptions are combined with the solar irradiance variability in the natural forcing experiment (Nat) preventing their disentangling. For the recent decades, CMIP6 Nat simulations do not show any significant change of the HC edges (Figure 6). However, the results of CMIP simulations are uncertain, because the overall effect of stratospheric volcanic aerosol (and of tropospheric dust in general) strongly depends on the prescribed optical properties that can lead to very different, and sometimes opposite, results.<sup>222–224</sup>

## Orbital forcing and glacial-to-interglacial cycles

The modulation of the distribution of insolation by periodic changes of Earth's orbital eccentricity, axial obliquity, and apsidal precession (with periodicities approximately of 100, 41, and 23 kyr, respectively) in concert with cryosphere and carbon cycle feedbacks<sup>225,226</sup> drives the Quaternary glacial to interglacial cycles.<sup>227–229</sup> The complex interplay between orbital forcing, CO<sub>2</sub> concentration, ice-sheet dynamics, and ocean circulation has affected the HC strength and width (see the section “The ITCZ latitude and cross-equatorial energy transport”).

During Quaternary interglacials, proxy and modeling evidence indicate orbitally induced climate conditions different from present day. During the early-to-mid Holocene (9.5–6 kyr BP) and the early Eemian (126 kyr BP) interglacials, the NH warming and enhanced interhemispheric insolation and SST gradients in the boreal summer (compared to preindustrial conditions) presumably led to stronger winter solstitial SH HC and NH monsoons, and a northward shift of the ITCZ, consistent with the relationships found in PMIP models (see the section “The ITCZ latitude and cross-equatorial energy transport” and Refs. 145, 230, 231). In the boreal winter, models indicate that reduced interhemispheric insolation asymmetries have led to weaker winter solstitial NH HC, SH monsoons, and equatorward shift of the ITCZ relative to preindustrial.<sup>231,232</sup>

PMIP simulations of LGM (~21 kyr BP) clearly show that the winter solstitial HC was stronger and narrower than in preindustrial conditions.<sup>105,108</sup> Literature also provides a consensus on an equatorward shift of the ITCZ.<sup>233</sup> During the glacial and cold episodes, such as the Younger Dryas (12.9–11.7 kyr BP) and Heinrich stadials, the complex interplay between orbital and CO<sub>2</sub> forcing, and ice-sheets dynamics presumably led to an AMOC slowdown.<sup>234,235</sup> Climate model simulations of the Heinrich stadials show decreased northward OHT and an associated equatorward shift of the ITCZ, weakening of the NH monsoons, and a relatively wetter climate in the SH.<sup>236</sup> Similar to other cold periods, reconstructions for the last glacial maximum show a southward shift of the ITCZ<sup>233</sup> and reinforced northeast trade winds.<sup>105,237</sup> Trade winds proxies of the HC during cold episodes are consistent with the response predicted in the section “Linking the ITCZ position with ocean heat transport, TOA flux, and SST”: cooling the NH relative to the SH shifts the ITCZ equatorward and strengthens the NH trade winds, while it weakens them in the SH.<sup>236</sup> Paleo-proxy and energetic considerations<sup>47</sup> show that the equatorward shift of the ITCZ was likely less than 1° at the LGM,<sup>47</sup> suggesting that inferences of large (up to 4°–5°) shifts from a single proxy may reflect localized changes.

## REGIONALITY OF THE HC

The section “The responses of the HC to natural and anthropogenic forcings” highlighted the hemispheric asymmetry as well as regional impacts of different forcings on the HC. This suggests that changes or absence of changes in the global HC due to a specific forcing may result

from a combination of additive or competing regional effects. Therefore, the global perspective is likely to miss important regional changes (addressed in this section) that have important environmental effects on precipitation and droughts.

## Characteristics of the regional HCs

The HC shown in Figure 2 does not resemble the circulation at any given longitude. Areas of ascent do not spread uniformly around the globe, rather they are strongly localized.<sup>58,64</sup> The seasonal cycle of the local MSF  $\psi(\lambda, \phi, p)$  at  $p = 500$  hPa (Figure 7, left panel) shows three centers of minima in the SH and maxima in the NH located near the equator above Africa, the Maritime Continent, and America. These minima/maxima in each hemisphere are meridionally separated by the zero contours of the MSF near the equator, which are associated with intense ascent and where the meridional gradient of  $\psi$  is strongest, concomitant with the ITCZ. The regions of intense ascent are zonally separated by a discontinuity near 60° E, 140° W, and 20° W and are marked by seasonal and regional variability. The strongest center is located above the Maritime Continent in the solstitial seasons and the weakest above Africa in the equinoctial seasons.

Wherever there is a tropical monsoon regime associated with deep convection and rising motion near the equator and descending motion in the subtropics, with equatorward flow near the surface and return flow in the upper troposphere, it is possible to define a regional HC.<sup>232,238,239</sup> This motivates a regional perspective of the HC, where Equation (3) is used to define  $\Psi_R(\phi, p)$  for three different regions (AsiaPac, EurAfr, and Americas, Figure 1) characterized by different morphology, land-sea patterns, monsoonal flow, and seasonally varying ITCZ.<sup>64</sup> This regionalization is consistent with a recent theoretical framework that describes the HC as the results of active tropical convection occurring over specific zones (Equatorial Africa, Indian Ocean and west Pacific, east Pacific, and Equatorial America) and enhanced during certain periods causing meridional circulations on longitudinally confined sectors.<sup>238,239</sup> All three regional HCs (Figure 1b–d) exhibit an overturning structure in both hemispheres, but with marked regional variability, which is associated with the different strengths of their respective ITCZ and rising branch (Figure 7). The AsiaPac HC is the strongest, while the EurAfr HC is the weakest. The width of the cells differs among the three regions especially in the NH where the AsiaPac cell extends far beyond the subtropical latitudes due to the strong Asian summer monsoon.<sup>238</sup> This is consistent with other studies that have described the zonal variations of subtropical margins using different metrics.<sup>13,32</sup> The results shown in Figures 7 (left panel) and 8 have been obtained using the most recent ECMWF reanalysis product ERA5 for the period 1979–2020 and confirm that the AsiaPac is stronger and wider than the other two HCs. The main features and the magnitude of the local MSF in the Asia-Pacific, Europe-Africa, America sectors and their seasonal variations are similar if a different (e.g., 1970–2014) period is considered or the former ERA-Interim reanalysis is adopted, and they are consistent with analog published climatologies.<sup>62</sup>

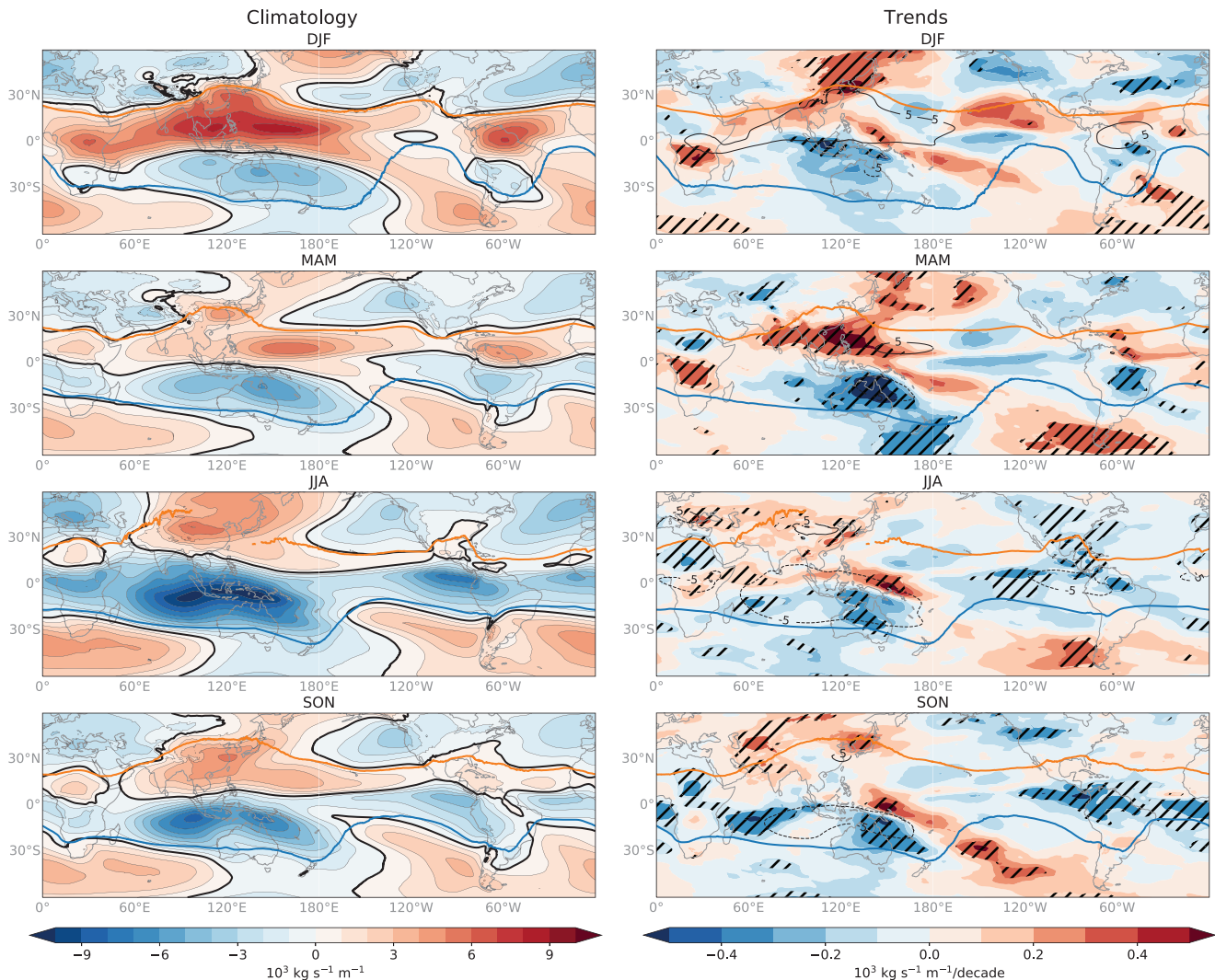


**FIGURE 7** Seasonal cycle of the local MSF at 500 hPa (left) and their long-term trend (right) derived from the ERA5 divergent meridional wind over the period 1979–2020. In the left column panels, the zero-contour is highlighted in black. In the right column panels, hatched areas denote values statistically significant to the 95% level and black solid/dashed contours show the  $\pm 5 \times 10^7 \text{ kg s}^{-1}$  MSF levels. In all panels, thick orange and blue lines indicate the local edges of the overturning circulation when they can be defined.

The intensity of the regional HC can be defined as the maximum of  $\Psi_R(\phi, p)$  between the equator and  $30^\circ$  latitude and its edge as the latitude where  $\Psi_R(\phi, p)$  is decreased to 25% poleward from its maximum value averaged between 400 and 700 hPa.<sup>64</sup> Though this threshold is subjective, its value is not critical and reducing it (e.g., to 10% as in Ref. 62) does not appreciably affect the results. The methodology adopted in Figure 7 fails to identify the edge of the HC NH only in the Asia-Pacific sector in the boreal summer in a zone around the west coast of the Pacific Ocean, but, depending on the adopted methodology, the definition of the HC edges may fail at several longitudes.<sup>62</sup> However, results are generally consistent at the longitudes where the edges are identified by the different methods and datasets. The seasonal cycle of the edge and intensity of the regional and global HC are presented in Figure 8. Both the edge and intensity of the regional HCs loosely follow the annual cycle of the global HC. According to the maps of the local MSF at 500 hPa (Figure 7), in the NH between May and August, the (summer solstitial) AsiaPac has no well-defined north-

ern limit. The occurrence of the maximum (minimum) extension of the Americas NH (SH) HC during the autumn (spring) equinoctial conditions might be an artifact caused by the criterion used for defining the edges; in this case, the HC is weak and its regional extension has an irregular shape. Note that the weighted average of the regional edges equals the global edge and the sum of the regional intensities equals the global intensity (Figure 8).

### Past and projected changes of the regional HCs under anthropogenic climate change

Here, we discuss changes of the HC that are marked by regionality and seasonality (e.g., Refs. 13, 58, 62) using the ERA5 data for the period 1979–2020 to support the discussion.<sup>1</sup>

<sup>1</sup> These data and results have not been previously published.

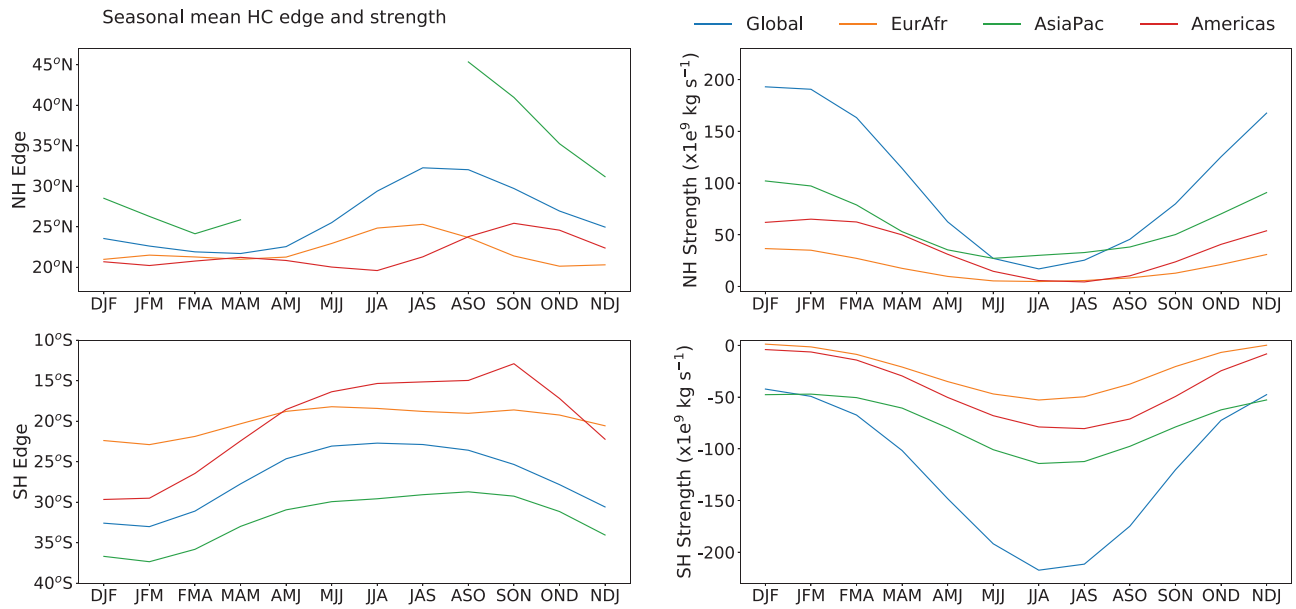


**FIGURE 8** Seasonal cycle (3-month running average) of the edge (left, in degrees of latitude) and strength (right, in  $\text{kg s}^{-1}$ ) of the three regional and global HCs for the Northern (top, NH) and Southern (bottom, SH) Hemisphere according to ERA5 and the 1979–2020 period. The regional HCs are Europe–Africa (EurAfr;  $20^\circ \text{W}$ – $65^\circ \text{E}$ , orange), Asia–Pacific (AsiaPac;  $65^\circ \text{E}$ – $140^\circ \text{W}$ , green), and Americas (Am  $140^\circ \text{W}$ – $20^\circ \text{W}$ , red). Missing values in the summer months for AsiaPac NH edge are due to the cell extending to the pole.

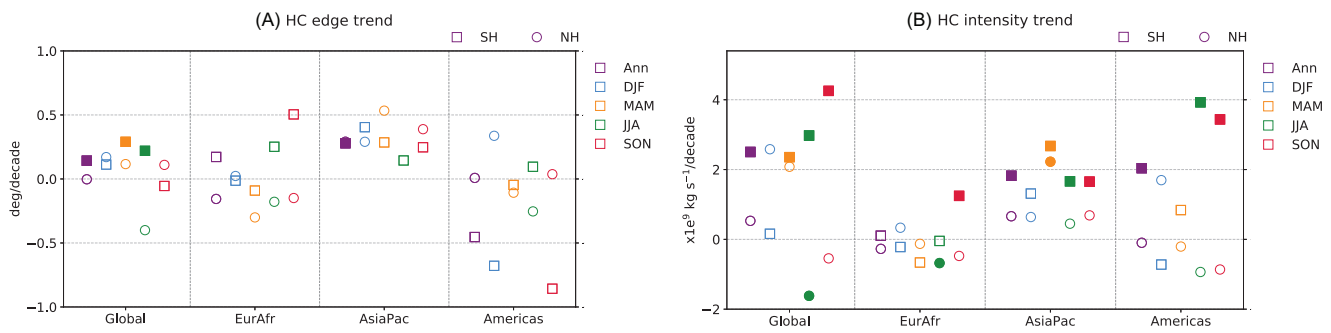


**FIGURE 9** ERA5 1979–2020 annual and seasonal trends in the edge (panel A) and strength (panel B) of the zonal mean and regional HCs. Trends in the NH/SH are indicated by open circles/squares, with values statistically significant (at the 95% confidence level) indicated by filled circles/squares. Positive values indicate expansion/strengthening.

Figure 9A shows the trends of the HC poleward edges adopting a 95% significance level. Global expansion is driven by the Asia-Pacific HC, which is the unique sector presenting positive values in all seasons and in both hemispheres, while in the Europe–Africa and America sectors, most values are negative. The statistically significant global expansion of the winter solstitial and autumn equinoctial SH HC results from nonsignificant trends that are positive in all sectors in winter, but only in the Asia-Pacific HC in autumn. At the annual scale, the statistically significant expansion of the SH HC results from the positive trend in the Asia-Pacific sector, only partially reduced by narrowing (statistically nonsignificant) in the America sector. There are no statistical significant trends of the NH HC.

Figure 9B shows strengthening of the HC, which is more robust in the SH than in the NH. The SH HC strengthening is driven mostly by

the intensification in the Asia-Pacific sector, which is significant in all seasons but summer. In the NH, weakening of the Europe–Africa and America sectors contrasts the strengthening of the Asia-Pacific sector in all seasons, leading to a significant weakening of the summer solstitial global NH HC. The agreement with Ref. 62 is partial as their results show HC strengthening in the America sector in all seasons.

Therefore, Figure 9 shows that the HC expansion and strengthening in the period 1979–2020 have not been zonally uniform, but actually contraction and weakening have occurred in many seasons for the Europe–Africa and America sectors. Further, natural variability prevents identifying statistically significant trends at regional scale in most sectors and seasons.

Breaking down the HC regional changes of Figure 9 to longitudinal scale by the analysis of the local  $\psi(\lambda, \phi, p)$  (Figure 7, right panel)

allows one to interpret the trends in Figure 9 in terms of sub-regional features. In most season, the expansion and strengthening of the AsiaPac SH HC is driven by its behavior over the Maritime Continent. The intensification of the winter SH HC in the Americas sector is reflected in a significant signal over south America and the East Pacific in Figure 7, while the interpretation of the trends over equatorial Africa is less clear. Many features that are present in Ref. 62 are confirmed in Figure 7 right panel, but in Figure 7, the intensification of the HC above America and the Indian Ocean in JJA are weaker and have a different spatial structure than in Ref. 62. Further, Ref. 58 shows SH winter solstitial trends different than in Ref. 62 above equatorial America and does not exhibit the significant intensification of the Asia-pacific SH HC that is evident in Figure 7, right panel. These disagreements can be partially explained by the different periods that have been adopted (1979–2017 for Ref. 62, 1979–2009 for Ref. 58, and 1979–2020 for Figure 7), as these trends are strongly affected by natural variability,<sup>62,166</sup> but it is also likely that structural issues can locally cause substantial differences between reanalyses (namely between ERA-Interim and ERA5).

Beside land–sea contrast and ocean circulations, a major role in the lack of zonal uniformity of past evolution of the HC is played by aerosol emissions, whose major sources have moved in the last few decades from North America and Western Europe to East Asia and tropical regions. In the regions of strong convection such as in monsoon areas and the ITCZ, the BC-induced surface cooling and tropospheric warming could have masked the effect of GHG forcing, and may have been responsible for regional impacts, such as Sahel drought, Indian monsoon weakening, and meridional shift of the East Asian rainfall pattern observed in the mid-20th century. In arid and hyper-arid areas collocated with the HC descending branch, the overall BC effect could have contributed to expansion of the subtropical dry zones and local increase of drought intensity.<sup>169,207,240</sup>

Dust, which has not been included in CMIP aerosol prescriptions,<sup>207</sup> absorbs solar radiation and absorbs/re-emits thermal infrared radiation<sup>241</sup> exerting a large influence on the energy budget of the dry subtropics, such as the Saharan and Arabian deserts. Over North Africa, the dust radiative effect strengthens the NH HC, inducing a slight northward shift of the ITCZ and increased precipitation.<sup>177</sup> However, global climate model simulations show a contrasting response of the tropical rain belt to dust forcing.<sup>242–245</sup> The disagreement may arise from uncertainties associated with different representation of dust optical properties, with large absorption producing a large negative net radiative effect and a positive impact on the hydrological cycle. On paleo-time scales, dust follows the long-term oscillations associated with glacial-interglacial cycles. During interglacial humid and more vegetated periods, such as the mid-Holocene, the HC is wider and stronger.<sup>105</sup> The dust reduction over the “Green Sahara” strengthens the vegetation–albedo feedback, increasing further the area and intensity of the African monsoon and the local HC.<sup>246</sup>

CMIP6 projections under the combined SSP3.0-RCP7.0 scenario show a northward shift of the ITCZ over eastern Africa and the Indian Ocean and a southward shift in the eastern Pacific and Atlantic Oceans and South America associated with changes in the divergent

atmospheric energy transport by 2100.<sup>247</sup> These shifts appear to be associated with meridional SST contrasts; in the Indian Ocean, higher SST warming is located in the northern subtropics, while in the eastern Pacific and Atlantic Oceans, it is located between 10° S and 5° N. The South Atlantic Convergence Zone is projected to shift southward in association with the deepening of the south Atlantic subtropical high,<sup>248</sup> while over Africa, the ITCZ is projected to shift northward associated with the deepening of the Saharan heat low.<sup>249</sup>

The multimodel mean local  $\psi(\lambda, \phi, p)$  weakens significantly at most longitudes<sup>62</sup> in an ensemble of simulations of CO<sub>2</sub> quadrupling. However, the widening signature is more complex. In the NH for the winter solstitial HC, widening is projected over the Middle East and the Western Pacific, while contraction is projected over Southwest America, North Atlantic, and East Asia (see also Ref. 232). The autumn widening of the equinoctial NH HC over east Pacific and Middle East results in a small NH HC widening. In contrast, SH widening is projected in all four seasons but is largely driven by widening over the East Pacific where the overturning circulation is weak. In summary, the projected regional effects of increasing GHG concentration and the trends in reanalyses present large discrepancies, that make the attribution of regional changes of the HC edges since 1979 to anthropogenic climate change problematic. The analysis of Ref. 13 suggests that the anthropogenic expansion of the tropical belt will emerge within this century only in few areas of the NH (the Mediterranean/Middle East and, to a lesser extent the Western Pacific).

## DISCUSSION AND CONCLUSIONS

Theoretical understanding of the HC dynamics generally considers the axisymmetric limit, in which eddies are not considered, and the eddy-driven small-Ro limit, in which extratropical processes strongly constrain the HC. In Earth's HC, the relevance of these limits is expected to differ at different points of the seasonal cycle. The axisymmetric scaling provided by the H&H model<sup>67</sup> represents a theoretical framework for the solstitial winter HC, since its response to the off-equatorial solar forcing is weakly influenced by eddies. The small-Ro limit<sup>78,84,85</sup> represents a theoretical framework more suitable than the axisymmetric theory for understanding the HC during equinoctial conditions, when its extension is associated with the activity of the mid-latitude eddies (controlled by the Eady growth rate) and the position of the storm track. In spite of theoretically different conditions for their validity, both frameworks have been applied in general to the HC. However, recent studies, which evidence the relevance of mid-latitude processes (and, therefore, of the small-Ro limit) both in equinoctial and solstitial conditions, suggest that the axisymmetric theory is not relevant for the HC width.<sup>81,109</sup>

The axisymmetric theory suggests that both HC width and strength increase with the troposphere depth and radiative equilibrium meridional temperature gradient, and that the strength also decreases with the thermal stratification in the tropics (see the section “Axisymmetric theory”). Small-Ro theory implies that the width is sensitive to changes in baroclinicity in the subtropics, implying that the latitude

of the HC edge shifts consistently with the meridional position of the mid-latitude storms track, and the HC strength is related to that of the eddy momentum flux divergence in the subtropics, implying that it varies with the intensity of the mid-latitude eddies (see the section "Axisymmetric theory").

Climate projections, largely driven by the radiative effects of the increasing GHG concentration, show significant expansion and weakening of the HC, which are consistent with the role of the troposphere depth and of the subtropical near-surface static stability, respectively (e.g., Refs. 44, 105, 165, 183, 250, 251) and/or increased static stability in the ascending branch with differences among the NH and SH.<sup>109, 112</sup> Since the parameters of the H&H scaling vary with global warming, the H&H model can be used to support the extension and weakening of the HC with the intensity of the anthropogenic climate change identified in PMIP3-CMIP5 numerical experiments.<sup>105</sup> The expansion of the HC is also supported by the small-Ro theoretical limit through the poleward migration of the storm track, increased static stability, and reduced meridional temperature gradients in the subtropics resulting from anthropogenic global warming.<sup>27, 28, 44, 99, 110</sup> These are the bases for the expectation of the future expansion and weakening of the winter HC, but with uncertainties on their magnitude, so that the climate change signal might not emerge from natural variability in the NH during the 21st century even in a high emission scenario.<sup>167</sup>

Energy budget considerations suggest that the tropical circulation weakens in response to the increase of gross moist stability of the tropical troposphere, but strengthens with increasing *NEI*, which are both effects caused by increasing GHG concentration. Climate models generally favor a decrease in HC strength with warming, although a strengthening cannot be ruled out either based on models or theoretical considerations, limiting the confidence on the future weakening of the HC.

Historical climate simulations and meteorological reanalyses suggest that an expansion of the HC has occurred in the recent decades (particularly of the winter solstitial HC). The quantitative agreement among the two sets of data is poor, with substantially smaller trends in simulations than in reanalyses (e.g., Refs. 26, 42, 98, 110, 160, 164, 252), but they can be reconciled accounting for the large role of natural variability that has approximately doubled the rate of tropical expansion from that expected from anthropogenic forcing alone.<sup>107, 167, 171</sup> Changes in the HC strength and their interpretation are uncertain. The HC has been mostly weakening in historical simulations of GHG<sup>164</sup> but mostly strengthening in reanalyses (as it is shown also the ERA5 data considered in this article) particularly in the SH. Using sea-level pressure gradients to estimate the change of the HC strength,<sup>253</sup> suggested that the NH HC has weakened over recent decades, and the weakening is attributable to anthropogenic emissions. The proposed explanations for these disagreements include structural climate model deficiencies, multidecadal variability,<sup>40, 168</sup> and/or possible artifacts in the reanalyses.<sup>160</sup> In general, there is a growing evidence that properly accounting for natural variability, climate model, and reanalysis results can be reconciled<sup>32, 166, 168, 170</sup> and, though the reanalyses contain structural problems and systematic errors,<sup>160–162</sup> these issues do not prevent a realistic reconstruction of the past HC evolution.

Variations of the HC are linked to multiple factors that have played a role in the recent decades. The widening caused by increasing GHG concentration has been further amplified by the contribution of the stratospheric ozone depletion (at least in the SH). The NH cooling produced by anthropogenic aerosols is expected to have exerted an effect opposite to GHGs that occurred mostly in the NH, but there are large uncertainties in the estimates of their individual effects. Solar irradiance and volcanic forcing in the 20th century have not produced any significant trend of the HC in climate simulations. In synthesis, there is a consensus among theoretical arguments, reanalyses, and climate model simulations that an expansion of the global HC has occurred in the recent decades, and that increasing GHG concentration and stratospheric ozone depletion have contributed to it. Consistently with these mechanisms, climate models project robust future HC expansion in the SH (but not in the NH), and robust future HC weakening in the NH (but not in the SH) as a result of the GHG increase and the recovery of stratospheric ozone (e.g., Ref. 112).

Energy budget considerations provide a background for understanding variations of the strength of the AHT and of the shift of the ITCZ, which are relatively recent topics (e.g., they were not highlighted in Ref. 22). The annual mean location of the ITCZ north of the equator and the associated southward atmospheric heat transport at the equator are consolidated features across different climates and in recent times. This is caused by the large northward OHT across the equator overcompensating for different signs of the TOA energy budget of the two hemispheres. Anthropogenic climate change is expected to increase *NEI* in the tropics and, therefore, to simultaneously shift the ITCZ equatorwards and increase the AHT. The magnitude of both effects is uncertain.

During the last 15 years, regional aspects of the HC have gained relevance as the global perspective has revealed its limitation for the full understanding of recent, past and future trends of the HC. A measure of this progress could be the comparison of the discussion in this article with respect to Ref. 22, published in 2004, where the importance of regional features had only begun to emerge. In fact, the global HC concept hides the fact that both ascending and descending motions are not zonally uniform and are concentrated above the three areas: Equatorial Africa, the Maritime Continent, and Equatorial America. While these three regional features, particularly the HC above the maritime continent, can be clearly identified in all seasons, the HC and an overturning circulation do not exist at all longitudes and seasons (e.g., in the central Pacific), and the identification of the edges might fail depending on the adopted method.

The identities of regional HCs and their different behaviors have become clear, also in terms of different past and future responses, including responses to forcings with regional characterizations (BC, volcanic and anthropogenic aerosols, tropospheric and stratospheric ozone) and regional responses to globally homogeneous forcing (anthropogenic GHG). The expansion of the Asia-Pacific circulation in the SH has been the dominant signal in the last few decades and is expected to play the same role in the future. Further, the OHT variations in the different ocean basins can determine zonal variations of the ITCZ shift whose sign may change depending on the basin. In fact,

simulations show a future northward shift of the ITCZ over Africa and the Indian Ocean, southward over the Atlantic, eastern Pacific, and Americas. The large differences between the regional responses of the HC to GHG and the trends observed in reanalyses in the last 40 years make the attribution of its recent regional evolution to anthropogenic climate change problematic,<sup>62</sup> and the signal might need several decades to emerge at regional scale, particularly in the NH.<sup>13</sup> Reducing the existing uncertainties on regional responses of the HC to increasing GHG and other factors is presently problematic because there are multiple forcing agents present with contrasting effects and likely strong model-dependency of results, which have shown major limitations in reproducing the regional evolution of the HC in the last decades.

Though the present theoretical understanding provides useful guidelines, interpretation of past variations (particularly at the regional scale) is still in part uncertain. CMIP5 and CMIP6 simulations do not capture well HC, ITCZ, and precipitation changes, suggesting the need of reducing structural model uncertainties. However, important progress has been obtained explaining a substantial fraction of recent trends to multidecadal natural variability. A possible way forward to better connect theory to observation and simulations would be to unify the energetic and momentum-based perspectives discussed in the sections “Dynamics of the HC” and “Links of the HC with the energy budget” to a more coherent theory for the HC. Further, an important direction for future work is to develop theoretical constraints on regional HCs.

#### AUTHOR CONTRIBUTIONS

All authors share credit for the content of the article, particularly of the final section. P.L. coordinated the review. M.S.S., D.F., R.D., and H.N. led the writing of the second, third, fourth, and fifth sections, respectively.

#### ACKNOWLEDGMENTS

R.D. was funded by the Deutsche Forschungsgemeinschaft (DFG, German Research Foundation) under Germany's Excellence Strategy - EXC 2037 Climate, Climatic Change, and Society (CLICCS) - Cluster of Excellence Hamburg, A4 African and Asian Monsoon Margins - Project Number: 390683824.

R.D. acknowledges financial support under the National Recovery and Resilience Plan (NRRP), Mission 4, Component 2, Investment 1.1, Call for tender No. 1409 published on 14.9.2022 by the Italian Ministry of University and Research (MUR), funded by the European Union - NextGenerationEU - Project Title: DROMEDAR, Future DROughts and ARidification in the MEDiterranean and ecological impacts - Project Code: P2022A3MFC - CUP: B53D2303355001 - CUP Master: E53D23021930001 - Grant Assignment Decree No. 1388 adopted on 01/09/2023 by the Italian Ministry of Ministry of University and Research (MUR).

M.S. acknowledges funding from the Australian Research Council through grants DE190100866, DP200102954, and CE170100023. H.N. is supported by the Northern Australian Climate Program (NACP, <https://www.nacp.org.au/>), funded by Meat and Livestock Australia,

the Queensland Government and the University of Southern Queensland.

The authors acknowledge Yan Xia and Yongyun Hu for providing data for producing Figure 6.

The authors are very grateful to Kevin Grise for the data preindustrial control data shown in Figure 5 and to Yan Xia for the data shown in Figures 5 and 6. We are indebted to an anonymous reviewer for comments and suggestions that have substantially contributed to the quality of this review article.

#### COMPETING INTERESTS

The authors have no competing interests to disclose.

#### ORCID

Piero Lionello  <https://orcid.org/0000-0002-0779-5681>

#### PEER REVIEW

The peer review history for this article is available at: <https://publons.com/publon/10.1111/nyas.15114>

#### REFERENCES

1. Bjerknes, J. (1966). A possible response of the atmospheric Hadley circulation to equatorial anomalies of ocean temperature. *Tellus*, 18(4), 820–829.
2. Liang, X.-Z., & Wang, W.-C. (1998). Associations between China monsoon rainfall and tropospheric jets. *Quarterly Journal of the Royal Meteorological Society*, 124(552), 2597–2623.
3. Hou, A. Y. (1998). Hadley circulation as a modulator of the extratropical climate. *Journal of the Atmospheric Sciences*, 55(14), 2437–2457.
4. Numaguti, A. (1993). Dynamics and energy balance of the Hadley circulation and the tropical precipitation zones: Significance of the distribution of evaporation. *Journal of the Atmospheric Sciences*, 50(13), 1874–1887.
5. Zhou, Y. P., Xu, K.-M., Sud, Y. C., & Betts, A. K. (2011). Recent trends of the tropical hydrological cycle inferred from Global Precipitation Climatology Project and International Satellite Cloud Climatology Project data. *Journal of Geophysical Research: Atmospheres*, 116(D9), D09101.
6. Fontaine, B., Roucou, P., Gaetani, M., & Marteau, R. (2011). Recent changes in precipitation, ITCZ convection and northern tropical circulation over North Africa (1979–2007). *International Journal of Climatology*, 31(5), 633–648.
7. Wodzicki, K. R., & Rapp, A. D. (2016). Long-term characterization of the Pacific ITCZ using TRMM, GPCP, and ERA-Interim. *Journal of Geophysical Research: Atmospheres*, 121(7), 3153–3170.
8. Lau, W. K., & Tao, W. (2020). Precipitation–radiation–circulation feedback processes associated with structural changes of the ITCZ in a warming climate during 1980–2014: An observational portrayal. *Journal of Climate*, 33(20), 8737–8749.
9. Charney, J. G. (1975). Dynamics of deserts and drought in the Sahel. *Quarterly Journal of the Royal Meteorological Society*, 101(428), 193–202.
10. Rodwell, M. J., & Hoskins, B. J. (1996). Monsoons and the dynamics of deserts. *Quarterly Journal of the Royal Meteorological Society*, 122(534), 1385–1404.
11. Scheff, J., & Frierson, D. M. W. (2012). Robust future precipitation declines in CMIP5 largely reflect the poleward expansion of model subtropical dry zones. *Geophysical Research Letters*, 39(18), L18704.
12. Burls, N. J., Blamey, R. C., Cash, B. A., Swenson, E. T., al Fahad, A., Bopape, M.-J. M., Straus, D. M., & Reason, C. J. (2019). The Cape Town

- "Day Zero" drought and Hadley cell expansion. *Nature Partner Journals Climate and Atmospheric Science*, 2(1), 1–8.
13. D'Agostino, R., Scambiatì, A. L., Jungclauss, J., & Lionello, P. (2020). Poleward shift of northern subtropics in winter: Time of emergence of zonal versus regional signals. *Geophysical Research Letters*, 47, e2020GL089325.
  14. Halley, E. (1687). An historical account of the trade winds, and monsoons, observable in the seas between and near the Tropicks, with an attempt to assign the physical cause of the said winds. *Philosophical Transactions of the Royal Society of London*, 16(183), 153–168.
  15. Hadley, G. (1735). VI. Concerning the cause of the general trade-winds. *Philosophical Transactions of the Royal Society of London*, 39(437), 58–62.
  16. Hildebrandsson, H. H., & de Bort, L. P. T. (1900). *Les bases de la météorologie dynamique: Historique-état de nos connaissances* (volume 2). Gauthier-Villars et fils.
  17. Lorenz, E. N. (1983). A history of prevailing ideas about the general circulation of the atmosphere. *Bulletin of the American Meteorological Society*, 64(7), 730–734.
  18. Lorenz, E. N., & Lorenz, F. N. (1967). *The nature and theory of the general circulation of the atmosphere* (volume 218). Geneva: World Meteorological Organization.
  19. Williams, J., Barry, R. G., & Washington, W. M. (1974). Simulation of the atmospheric circulation using the NCAR global circulation model with ice age boundary conditions. *Journal of Applied Meteorology and Climatology*, 13(3), 305–317.
  20. Bryson, R. A. (1974). A perspective on climatic change. *Science*, 184(4138), 753–760.
  21. Imbrie, J., & Imbrie, J. Z. (1980). Modeling the climatic response to orbital variations. *Science*, 207(4434), 943–953.
  22. Diaz, H. F., & Bradley, R. S. (2004). *The Hadley circulation: Present, past and future*. Springer.
  23. Ma, J., Chadwick, R., Seo, K.-H., Dong, C., Huang, G., Foltz, G. R., & Jiang, J. H. (2018). Responses of the tropical atmospheric circulation to climate change and connection to the hydrological cycle. *Annual Review of Earth and Planetary Sciences*, 46, 549–580.
  24. Rind, D., & Perlwitz, J. (2004). The response of the Hadley circulation to climate changes, past and future. In H. F. Diaz & R. S. Bradley (Eds.), *The Hadley circulation: Present, past and future* (pp. 399–435). Springer.
  25. Quan, X.-W., Diaz, H. F., & Hoerling, M. P. (2004). Change in the tropical Hadley cell since 1950. In H. F. Diaz & R. S. Bradley (Eds.), *The Hadley circulation: Present, past and future* (pp. 85–120). Springer.
  26. Hu, Y., & Fu, Q. (2007). Observed poleward expansion of the Hadley circulation since 1979. *Atmospheric Chemistry and Physics*, 7(19), 5229–5236.
  27. Previdi, M., & Liepert, B. G. (2007). Annular modes and Hadley cell expansion under global warming. *Geophysical Research Letters*, 34(22), L22701.
  28. Seidel, D. J., Fu, Q., Randel, W. J., & Reichler, T. J. (2008). Widening of the tropical belt in a changing climate. *Nature Geoscience*, 1, 21–24.
  29. Birner, T., Davis, S. M., & Seidel, D. J. (2014). The changing width of earth's tropical belt. *Physics Today*, 67(12), 38–44.
  30. Lucas, C., Timbal, B., & Nguyen, H. (2014). The expanding tropics: A critical assessment of the observational and modeling studies. *Wiley Interdisciplinary Reviews: Climate Change*, 5(1), 89–112.
  31. Staten, P. W., Lu, J., Grise, K. M., Davis, S. M., & Birner, T. (2018). Re-examining tropical expansion. *Nature Climate Change*, 8, 768–775.
  32. Staten, P. W., Grise, K. M., Davis, S. M., Karlsruks, K. B., Waugh, D. W., Maycock, A. C., Fu, Q., Cook, K., Adam, O., Simpson, I. R., Allen, R. J., Rosenlof, K., Chen, G., Ummenhofer, C. C., Quan, X.-W., Kossin, J. P., Davis, S.-W., & ando Son, Nicholas A. (2020). Tropical widening: From global variations to regional impacts. *Bulletin of the American Meteorological Society*, 101(6), E897–E904.
  33. Oort, A. H., & Rasmusson, E. M. (1970). On the annual variation of the monthly mean meridional circulation. *Monthly Weather Review*, 98(6), 423–442.
  34. Oort, A. H., & Yienger, J. J. (1996). Observed interannual variability in the Hadley circulation and its connection to ENSO. *Journal of Climate*, 9(11), 2751–2767.
  35. Palmén, E., & Vuorela, L. A. (1963). On the mean meridional circulations in the Northern Hemisphere during the winter season. *Quarterly Journal of the Royal Meteorological Society*, 89(379), 131–138.
  36. Vuorela, L. A., & Tuominen, I. (1964). On the mean zonal and meridional circulations and the flux of moisture in the Northern Hemisphere during the summer season. *Pure and Applied Geophysics*, 57, 167–180.
  37. Johanson, C. M., & Fu, Q. (2009). Hadley cell widening: Model simulations versus observations. *Journal of Climate*, 22(10), 2713–2725.
  38. Davis, S. M., & Rosenlof, K. H. (2012). A multidagnostic intercomparison of tropical-width time series using reanalyses and satellite observations. *Journal of Climate*, 25(4), 1061–1078.
  39. Chen, J., & Bordoni, S. (2014). Orographic effects of the Tibetan Plateau on the East Asian summer monsoon: An energetic perspective. *Journal of Climate*, 27(8), 3052–3072.
  40. Davis, N. A., & Davis, S. M. (2018). Reconciling Hadley cell expansion trend estimates in reanalyses. *Geophysical Research Letters*, 45(20), 11–439.
  41. Adam, O., Grise, K. M., Staten, P., Simpson, I. R., Davis, S. M., Davis, N. A., Waugh, D. W., Birner, T., & Ming, A. (2018). The TropD software package (v1): Standardized methods for calculating tropical-width diagnostics. *Geoscientific Model Development*, 11(10), 4339–4357.
  42. Hu, Y., & Zhou, C. (2010). Decadal changes in the Hadley circulation. *Advances in Geosciences*, 16, 61.
  43. Chen, S. and Wei, K., Chen, W., & Song, L. (2014). Regional changes in the annual mean Hadley circulation in recent decades. *Journal of Geophysical Research: Atmospheres*, 119, 7815–7832.
  44. Lu, J., Vecchi, G. A., & Reichler, T. (2007). Expansion of the Hadley cell under global warming. *Geophysical Research Letters*, 34(6), L06805.
  45. Davis, N., & Birner, T. (2016). Climate model biases in the width of the tropical belt. *Journal of Climate*, 29(5), 1935–1954.
  46. Baldassare, D., Reichler, T., Plink-Björklund, P., & Slawson, J. (2023). Large uncertainty in observed estimates of tropical width from the meridional stream function. *Weather and Climate Dynamics*, 4(2), 531–541.
  47. McGee, D., Donohoe, A., Marshall, J., & Ferreira, D. (2014). Changes in ITCZ location and cross-equatorial heat transport at the Last Glacial Maximum, Heinrich Stadial 1, and the mid-Holocene. *Earth and Planetary Science Letters*, 390, 69–79.
  48. Waugh, D. W., Grise, K. M., Seviour, W. J. M., Davis, S. M., Davis, N., Adam, O., Son, S.-W., Simpson, I. R., Staten, P. W., Maycock, A. C., Ummenhofer, C. C., Birner, T., & Ming, A. (2018). Revisiting the relationship among metrics of tropical expansion. *Journal of Climate*, 31(18), 7565–7581.
  49. Davis, N., & Birner, T. (2017). On the discrepancies in tropical belt expansion between reanalyses and climate models and among tropical belt width metrics. *Journal of Climate*, 30(4), 1211–1231.
  50. Dima, I. M., & Wallace, J. M. (2003). On the seasonality of the Hadley cell. *Journal of the Atmospheric Sciences*, 60, 1522–1527.
  51. Luo, J.-J., Sasaki, W., & Masumoto, Y. (2012). Indian Ocean warming modulates Pacific climate change. *Proceedings of the National Academy of Sciences*, 109(46), 18701–18706.
  52. McGregor, S., Timmermann, A., Stuecker, M. F., England, M. H., Merrifield, M., Jin, F.-F., & Chikamoto, Y. (2014). Recent Walker circulation strengthening and Pacific cooling amplified by Atlantic warming. *Nature Climate Change*, 4(10), 888–892.

53. Craig, P. M., Ferreira, D., & Methven, J. (2020). Monsoon-induced zonal asymmetries in moisture transport cause anomalous Pacific precipitation minus evaporation. *Geophysical Research Letters*, 47(18), e2020GL088659.
54. Trenberth, K. E., Stepaniak, D. P., & Caron, J. M. (2000). The global monsoon as seen through the divergent atmospheric circulation. *Journal of Climate*, 13(22), 3969–3993.
55. Hoskins, B., Yang, G.-Y., & Fonseca, R. (2020). The detailed dynamics of the June–August Hadley cell. *Quarterly Journal of the Royal Meteorological Society*, 146(727), 557–575.
56. Hoskins, B., & Yang, G.-Y. (2021). The detailed dynamics of the Hadley cell. Part II: December–February. *Journal of Climate*, 34(2), 805–823.
57. Schwendike, J., Govekar, P., Reeder, M. J., Wardle, R., Berry, G. J., & Jakob, C. (2014). Local partitioning of the overturning circulation in the tropics and the connection to the Hadley and Walker circulations. *Journal of Geophysical Research: Atmospheres*, 119(3), 1322–1339.
58. Schwendike, J., Berry, G. J., Reeder, M. J., Jakob, C., Govekar, P., & Wardle, R. (2015). Trends in the local Hadley and local Walker circulations. *Journal of Geophysical Research: Atmospheres*, 120(15), 7599–7618.
59. Kim, Y. H., Min, S. K., Son, S. W., & Choi, J. (2017). Attribution of the local Hadley cell widening in the Southern Hemisphere. *Geophysical Research Letters*, 44, 1015–1024.
60. Studholme, J., & Gulev, S. (2018). Concurrent changes to Hadley circulation and the meridional distribution of tropical cyclones. *Journal of Climate*, 31(11), 4367–4389.
61. Galanti, E., Raiter, D., Kaspi, Y., & Tziperman, E. (2022). Spatial patterns of the tropical meridional circulation: Drivers and teleconnections. *Journal of Geophysical Research: Atmospheres*, 127(2), e2021JD035531.
62. Staten, P. W., Grise, K. M., Davis, S. M., Karnauskas, K., & Davis, N. (2019). Regional widening of tropical overturning: Forced change, natural variability, and recent trends. *Journal of Geophysical Research: Atmospheres*, 124(12), 6104–6119.
63. Karnauskas, K. B., & Ummenhofer, C. C. (2014). On the dynamics of the Hadley circulation and subtropical drying. *Climate Dynamics*, 42, 2259–2269.
64. Nguyen, H., Hendon, H. H., Lim, E.-P., Boschhat, G., Maloney, E., & Timbal, B. (2018). Variability of the extent of the Hadley circulation in the Southern Hemisphere: A regional perspective. *Climate Dynamics*, 50, 129–142.
65. Sun, Y., Li, L. Z. X., Ramstein, G., Zhou, T., Tan, N., Kageyama, M., & Wang, S. (2019). Regional meridional cells governing the interannual variability of the Hadley circulation in boreal winter. *Climate Dynamics*, 52, 831–853.
66. Hersbach, H., Bell, B., Berrisford, P., Hirahara, S., Horányi, A., Muñoz-Sabater, J., Nicolas, J., Peubey, C., Radu, R., Schepers, D., Simmons, A., Soci, C., Abdalla, S., Abellan, X., Balsamo, G., Bechtold, P., Biavati, G., Bidlot, J., Bonavita, M., ... Thépaut, J.-N. (2020). The ERA5 global reanalysis. *Quarterly Journal of the Royal Meteorological Society*, 146(730), 1999–2049.
67. Held, I. M., & Hou, A. Y. (1980). Nonlinear axially symmetric circulations in a nearly inviscid atmosphere. *Journal of the Atmospheric Sciences*, 37, 515–533.
68. Walker, C. C., & Schneider, T. (2006). Eddy influences on Hadley circulations: Simulations with an idealized GCM. *Journal of the Atmospheric Sciences*, 63, 3333–3350.
69. Singh, M. S. (2019). Limits on the extent of the solstitial Hadley cell: The role of planetary rotation. *Journal of the Atmospheric Sciences*, 76, 1989–2004.
70. Hill, S. A., Bordoni, S., & Mitchell, J. L. (2019). Axisymmetric constraints on cross-equatorial Hadley cell extent. *Journal of the Atmospheric Sciences*, 76, 1547–1564.
71. Guendelman, I., & Kaspi, Y. (2018). An axisymmetric limit for the width of the Hadley cell on planets with large obliquity and long seasonality. *Geophysical Research Letters*, 45, 13–213.
72. Schneider, T., & Bordoni, S. (2008). Eddy-mediated regime transitions in the seasonal cycle of a Hadley circulation and implications for monsoon dynamics. *Journal of the Atmospheric Sciences*, 65(3), 915–934.
73. Schneider, E. K. (1977). Axially symmetric steady-state models of the basic state for instability and climate studies. Part II. Nonlinear calculations. *Journal of the Atmospheric Sciences*, 34(2), 280–296.
74. Satoh, M. (1994). Hadley circulations in radiative-convective equilibrium in an axially symmetric atmosphere. *Journal of the Atmospheric Sciences*, 51(13), 1947–1968.
75. Fang, M., & Tung, K. K. (1996). A simple model of nonlinear Hadley circulation with an ITCZ: Analytic and numerical solutions. *Journal of the Atmospheric Sciences*, 53, 1241–1261.
76. Fang, M., & Tung, K. K. (1999). Time-dependent nonlinear Hadley circulation. *Journal of the Atmospheric Sciences*, 56, 1797–1807.
77. Caballero, R., Pierrehumbert, R. T., & Mitchell, J. L. (2008). Axisymmetric, nearly inviscid circulations in non-condensing radiative-convective atmospheres. *Quarterly Journal of the Royal Meteorological Society*, 134, 1269–1285.
78. Schneider, E. K., & Lindzen, R. S. (1977). Axially symmetric steady-state models of the basic state for instability and climate studies. Part I. Linearized calculations. *Journal of the Atmospheric Sciences*, 34(2), 263–279.
79. Frierson, D. M., Lu, J., & Chen, G. (2007). Width of the Hadley cell in simple and comprehensive general circulation models. *Geophysical Research Letters*, 34(18), L18804.
80. Lindzen, R. S., & Hou, A. V. (1988). Hadley circulations for zonally averaged heating centered off the equator. *Journal of the Atmospheric Sciences*, 45(17), 2416–2427.
81. Levine, X. J., & Schneider, T. (2015). Baroclinic eddies and the extent of the Hadley circulation: An idealized GCM study. *Journal of the Atmospheric Sciences*, 72, 2744–2761.
82. Held, I. M. (2000). The general circulation of the atmosphere. In *Proceedings of Geophysical Fluid Dynamics Program* (pp. 1–54). Woods Hole Oceanographic Institution.
83. Randel, W. J., & Held, I. M. (1991). Phase speed spectra of transient eddy fluxes and critical layer absorption. *Journal of the Atmospheric Sciences*, 48(5), 688–697.
84. Kuo, H. L. (1956). Forced and free meridional circulations in the atmosphere. *Journal of Meteorological Research*, 13, 561–568.
85. Eliassen, A. (1951). Slow thermally or frictionally controlled meridional circulation in a circular vortex. *Astrophysica Norvegica*, 5, 19.
86. Kim, H.-K., & Lee, S. (2001). Hadley cell dynamics in a primitive equation model. Part II: Nonaxisymmetric flow. *Journal of the Atmospheric Sciences*, 58, 2859–2871.
87. Becker, E., Schmitz, G., & Geprägs, R. (1997). The feedback of midlatitude waves onto the Hadley cell in a simple general circulation model. *Tellus*, 49A, 182–199.
88. Walker, C. C., & Schneider, T. (2005). Response of idealized Hadley circulations to seasonally varying heating. *Geophysical Research Letters*, 32, L06813.
89. Singh, M. S., & Kuang, Z. (2016). Exploring the role of eddy momentum fluxes in determining the characteristics of the equinoctial Hadley circulation: Fixed-SST simulations. *Journal of the Atmospheric Sciences*, 73(6), 2427–2444.
90. Singh, M. S., Kuang, Z., & Tian, Y. (2017). Eddy influences on the strength of the Hadley circulation: Dynamic and thermodynamic perspectives. *Journal of the Atmospheric Sciences*, 74(2), 467–486.
91. Davis, N. A., & Birner, T. (2019). Eddy influences on the Hadley circulation. *Journal of Advances in Modeling Earth Systems*, 11, 1563–1581.

92. Satoh, M., Shiobara, M., & Takahashi, M. (1995). Hadley circulations and their rôles in the global angular momentum budget in two- and three-dimensional models. *Tellus*, 47(5), 548–560.
93. Moon, H., & Ha, K.-J. (2020). Distinguishing changes in the Hadley circulation edge. *Theoretical and Applied Climatology*, 139(3), 1007–1017.
94. Kang, S. M., & Polvani, L. M. (2011). The interannual relationship between the latitude of the eddy-driven jet and the edge of the Hadley cell. *Journal of Climate*, 24, 563–568.
95. Kidston, J., Cairns, C. W., & Paga, P. (2013). Variability in the width of the tropics and the annular modes. *Geophysical Research Letters*, 40, 2328–2332.
96. Ceppi, P., & Hartmann, D. L. (2013). On the speed of the eddy-driven jet and the width of the Hadley cell in the Southern Hemisphere. *Journal of Climate*, 26, 3450–3465.
97. Staten, P. W., & Reichler, T. (2014). On the ratio between shifts in the eddy-driven jet and the Hadley cell edge. *Climate Dynamics*, 42, 1229–1242.
98. Nguyen, H., Evans, A., Lucas, C., Smith, I., & Timbal, B. (2013). The Hadley circulation in reanalyses: Climatology, variability, and change. *Journal of Climate*, 26(10), 3357–3376.
99. Lu, J., Chen, G., & Frierson, D. M. (2008). Response of the zonal mean atmospheric circulation to El Niño versus global warming. *Journal of Climate*, 21, 5835–5851.
100. Bordoni, S., & Schneider, T. (2008). Monsoons as eddy-mediated regime transitions of the tropical overturning circulation. *Nature Geoscience*, 1, 515–519.
101. Bordoni, S., & Schneider, T. (2010). Regime transitions of steady and time-dependent Hadley circulations: Comparison of axisymmetric and eddy-permitting simulations. *Journal of the Atmospheric Sciences*, 67, 1643–1654.
102. Caballero, R. (2007). Role of eddies in the interannual variability of Hadley cell strength. *Geophysical Research Letters*, 34, L22705.
103. Caballero, R. (2008). Hadley cell bias in climate models linked to extratropical eddy stress. *Geophysical Research Letters*, 35, L18709.
104. Seo, K.-H., Frierson, D. M. W., & Son, J.-H. (2014). A mechanism for future changes in Hadley circulation strength in CMIP5 climate change simulations. *Geophysical Research Letters*, 41(14), 5251–5258.
105. D'Agostino, R., Lionello, P., Adam, O., & Schneider, T. (2017). Factors controlling Hadley circulation changes from the Last Glacial Maximum to the end of the 21st century. *Geophysical Research Letters*, 44(16), 8585–8591.
106. Vallis, G. K., Zurita-Gotor, P., Cairns, C., & Kidston, J. (2015). Response of the large-scale structure of the atmosphere to global warming. *Quarterly Journal of the Royal Meteorological Society*, 141(690), 1479–1501.
107. Adam, O., Schneider, T., & Harnik, N. (2014). Role of changes in mean temperatures versus temperature gradients in the recent widening of the Hadley circulation. *Journal of Climate*, 27, 7450–7461.
108. Son, S.-W., Kim, S.-Y., & Min, S.-K. (2018). Widening of the Hadley cell from Last Glacial Maximum to future climate. *Journal of Climate*, 31(1), 267–281.
109. Chemke, R., & Polvani, L. M. (2019). Exploiting the abrupt 4× CO<sub>2</sub> scenario to elucidate tropical expansion mechanisms. *Journal of Climate*, 32(3), 859–875.
110. Nguyen, H., Lucas, C., Evans, A., Timbal, B., & Hanson, L. (2015). Expansion of the Southern Hemisphere Hadley cell in response to greenhouse gas forcing. *Journal of Climate*, 28, 8067–8077.
111. Davis, N. A., & Birner, T. (2021). Eddy-mediated Hadley cell expansion due to axisymmetric angular momentum adjustment to greenhouse gas forcings. *Journal of the Atmospheric Sciences*, 79(1), 141–159.
112. Chemke, R., & Polvani, L. (2021). Elucidating the mechanisms responsible for Hadley cell weakening under 4× CO<sub>2</sub> forcing. *Geophysical Research Letters*, 48(3), e2020GL090348.
113. Levine, X. J., & Schneider, T. (2011). Response of the Hadley circulation to climate change in an aquaplanet GCM coupled to a simple representation of ocean heat transport. *Journal of the Atmospheric Sciences*, 68, 769–783.
114. Qiao, Y., Huang, W., & Jian, M. (2012). Impacts of El Niño–Southern Oscillation and local sea surface temperature on moisture source in Asian–Australian monsoon region in boreal summer. *Aquatic Ecosystem Health & Management*, 15, 31–38.
115. Gadgil, S. (2018). The monsoon system: Land–sea breeze or the ITCZ? *Journal of Earth System Science*, 127, 1.
116. Geen, R., Bordoni, S., Battisti, D. S., & Hui, K. L. (2020). Monsoons, ITCZs, and the concept of the global monsoon. *Reviews of Geophysics*, 58, e2020RG000700. <https://doi.org/10.1029/2020RG000700>
117. Cook, K. H. (2003). Role of continents in driving the Hadley cells. *Journal of the Atmospheric Sciences*, 60(7), 957–976.
118. Plumb, R. A., & Hou, A. Y. (1992). The response of a zonally symmetric atmosphere to subtropical thermal forcing: Threshold behavior. *Journal of the Atmospheric Sciences*, 49(19), 1790–1799.
119. Shaw, T. A. (2014). On the role of planetary-scale waves in the abrupt seasonal transition of the Northern Hemisphere general circulation. *Journal of the Atmospheric Sciences*, 71(5), 1724–1746.
120. Geen, R., Lambert, F. H., & Vallis, G. K. (2018). Regime change behavior during Asian monsoon onset. *Journal of Climate*, 31, 3327–3348.
121. Boos, W. R., & Emanuel, K. A. (2008). Wind–evaporation feedback and abrupt seasonal transitions of weak, axisymmetric Hadley circulations. *Journal of the Atmospheric Sciences*, 65, 2194–2214.
122. Ma, D., Sobel, A. H., Kuang, Z., Singh, M. S., & Nie, J. (2019). A moist entropy budget view of the South Asian summer monsoon onset. *Geophysical Research Letters*, 46, 4476–4484.
123. Faulk, S., Mitchell, J., & Bordoni, S. (2017). Effects of rotation rate and seasonal forcing on the ITCZ extent in planetary atmospheres. *Journal of the Atmospheric Sciences*, 74, 665–678.
124. Geen, R., Lambert, F. H., & Vallis, G. K. (2019). Processes and timescales in onset and withdrawal of “aquaplanet monsoons”. *Journal of the Atmospheric Sciences*, 76, 2357–2373.
125. Hill, S. A., Bordoni, S., & Mitchell, J. L. (2022). A theory for the Hadley cell descending and ascending edges throughout the annual cycle. *Journal of the Atmospheric Sciences*, 79(10), 2515–2528.
126. Seth, A., Rauscher, S. A., Rojas, M., Giannini, A., & Camargo, S. J. (2011). Enhanced spring convective barrier for monsoons in a warmer world? *Climatic Change*, 104, 403–414.
127. Chou, C., & Neelin, J. D. (2004). Mechanisms of global warming impacts on regional tropical precipitation. *Journal of Climate*, 17, 2688–2701.
128. Held, I. (2001). The partitioning of the poleward energy transport between the tropical ocean and atmosphere. *Journal of Atmospheric Sciences*, 58, 943–948.
129. Czaja, A., & Marshall, J. C. (2006). The partitioning of poleward heat transport between the atmosphere and ocean. *Journal of Atmospheric Sciences*, 63, 1498–1511.
130. Graversen, R., & Burtu, M. (2016). Arctic amplification enhanced by latent energy transport of atmospheric planetary waves. *Journal of the Royal Meteorological Society*, 142(698), 2046–2054.
131. Peixoto, J., & Oort, A. (1992). *Physics of climate*. American Institute of Physics.
132. Armour, K. C., Siler, N., Donohoe, A., & Roe, G. H. (2019). Meridional atmospheric heat transport constrained by energetics and mediated by large-scale diffusion. *Journal of Climate*, 32(12), 3655–3680.
133. Donohoe, A., Marshall, J., Ferreira, D., & McGee, D. (2013). The relationship between ITCZ location and cross equatorial atmospheric heat transport; From the seasonal cycle to the Last Glacial Maximum. *Journal of Climate*, 26, 3597–3618.
134. Neelin, J. D., & Held, I. M. (1987). Modeling tropical convergence based on the moist static energy budget. *Monthly Weather Review*, 115(1), 3–12.

135. Yu, J.-Y., Chou, C., & Neelin, J. D. (1998). Estimating the gross moist stability of the tropical atmosphere. *Journal of the Atmospheric Sciences*, 55(8), 1354–1372.
136. Raymond, D. J., Sessions, S. L., Sobel, A. H., & Fuchs, Ž. (2009). The mechanics of gross moist stability. *Journal of Advances in Modeling Earth Systems*, 1–9.
137. Chou, C., Wu, T.-C., & Tan, P.-H. (2013). Changes in gross moist stability in the tropics under global warming. *Climate Dynamics*, 41, 2481–2496.
138. Inoue, K., & Back, L. E. (2017). Gross moist stability analysis: Assessment of satellite-based products in the GMS plane. *Journal of the Atmospheric Sciences*, 74(6), 1819–1837.
139. Hill, S. A., Ming, Y., & Held, I. M. (2015). Mechanisms of forced tropical meridional energy flux change. *Journal of Climate*, 28(5), 1725–1742.
140. Wills, R. C., Levine, X. J., & Schneider, T. (2017). Local energetic constraints on Walker circulation strength. *Journal of the Atmospheric Sciences*, 74(6), 1907–1922.
141. Chou, C., & Chen, C.-A. (2010). Depth of convection and the weakening of tropical circulation in global warming. *Journal of Climate*, 23, 3019–3030.
142. Lucarini, V., & Ragone, F. (2011). Energetics of climate models: Net energy balance and meridional enthalpy transport. *Reviews of Geophysics*, 49(1), RG1001.
143. Schneider, T., Bischoff, T., & Haug, G. H. (2014). Migrations and dynamics of the intertropical convergence zone. *Nature*, 513, 45–53.
144. Philander, S. G. H., Gu, D., Lambert, G., Li, T., Halpern, D., Lau, N.-C., & Pacanowski, R. C. (1996). Why the ITCZ is mostly north of the equator. *Journal of Climate*, 9(12), 2958–2972.
145. D'Agostino, R., Bader, J., Bordoni, S., Ferreira, D., & Jungclaus, J. (2019). Northern Hemisphere monsoon response to mid-Holocene orbital forcing and greenhouse gas-induced global warming. *Geophysical Research Letters*, 46(3), 1591–1601.
146. Frierson, D. M., & Hwang, Y.-T. (2012). Extratropical influence on ITCZ shifts in slab ocean simulations of global warming. *Journal of Climate*, 25(2), 720–733.
147. Marshall, J., Donohoe, A., Ferreira, D., & McGee, D. (2013). The ocean's role in setting the mean position of the atmosphere's ITCZ. *Climate Dynamics*, 42, 1967–1979.
148. Liu, C., Allan, R. P., Mayer, M., Hyder, P., Desbruyeres, D., Cheng, L., Xu, J., Xu, F., & Zhang, Y. (2020). Variability in the global energy budget and transports 1985–2017. *Climate Dynamics*, 55, 3381–3396.
149. Lembo, V., Folini, D., Wild, M., & Lionello, P. (2019). Inter-hemispheric differences in energy budgets and cross-equatorial transport anomalies during the 20th century. *Climate Dynamics*, 53(1), 115–135.
150. Trenberth, K. E., & Fasullo, J. T. (2017). Atlantic meridional heat transports computed from balancing Earth's energy locally. *Geophysical Research Letters*, 44(4), 1919–1927.
151. Forget, G., & Ferreira, D. (2019). Global ocean heat transport dominated by heat export from the tropical Pacific. *Nature Geoscience*, 12, 351–354.
152. Ferreira, D., Cessi, P., Coxall, H. K., de Boer, A., Dijkstra, H. A., Drijfhout, S. S., Eldevik, T., Harnik, N., McManus, J. F., Marshall, D. P., Nilsson, J., Roquet, F., Schneider, T., & Wills, R. C. (2018). Atlantic-Pacific asymmetry in deep-water formation. *Annual Review of Earth and Planetary Sciences*, 46, 327–352.
153. Frierson, D. M., Hwang, Y.-T., Fučkar, N. S., Seager, R., Kang, S. M., Donohoe, A., Maroon, E. A., Liu, X., & Battisti, D. S. (2013). Contribution of ocean overturning circulation to tropical rainfall peak in the Northern Hemisphere. *Nature Geoscience*, 6(11), 940–944.
154. Broccoli, A. J., Dahl, K. A., & Stouffer, R. J. (2006). Response of the ITCZ to Northern Hemisphere cooling. *Geophysical Research Letters*, 33, L01702.
155. Kang, S. M., Held, I. M., & Xie, S. (2014). Contrasting the tropical responses to zonally asymmetric extratropical and tropical thermal forcing. *Climate Dynamics*, 42, 2033–2043.
156. Kang, S. M., Held, I. M., Frierson, D. M., & Zhao, M. (2008). The response of the ITCZ to extratropical thermal forcing: Idealized slab-ocean experiments with a GCM. *Journal of Climate*, 21(14), 3521–3532.
157. Moreno-Chamarro, E., Ferreira, D., & Marshall, J. (2020). Polar phasing and cross-equatorial heat transfer following a simulated abrupt NH warming of a glacial climate. *Paleoceanography and Paleoclimatology*, 35, e2019PA003810.
158. Green, B., Marshall, J., & Campin, J.-M. (2019). The 'sticky' ITCZ: Ocean-moderated ITCZ shifts. *Climate Dynamics*, 53(1), 1–19.
159. Liu, J., Song, M., Hu, Y., & Ren, X. (2012). Changes in the strength and width of the Hadley circulation since 1871. *Climate of the Past*, 8(4), 1169–1175.
160. D'Agostino, R., & Lionello, P. (2017). Evidence of global warming impact on the evolution of the Hadley circulation in ECMWF centennial reanalyses. *Climate Dynamics*, 48(9–10), 3047–3060.
161. Mitas, C. M., & Clement, A. (2006). Recent behavior of the Hadley cell and tropical thermodynamics in climate models and reanalyses. *Geophysical Research Letters*, 33(1), L01810.
162. Chemke, R., & Polvani, L. M. (2019). Opposite tropical circulation trends in climate models and in reanalyses. *Nature Geoscience*, 12(7), 528–532.
163. Dee, D. P., Uppala, S. M., Simmons, A. J., Berrisford, P., Poli, P., Kobayashi, S., Andrae, U., Balmaseda, M., Balsamo, G., Bauer, P., Bechtold, P., Beljaars, A. C. M., van de Berg, L., Bidlot, J., Bormann, N., Delsol, C., Dragani, R., Fuentes, M., Geer, A. J., ... Vitart, F. (2011). The era-interim reanalysis: Configuration and performance of the data assimilation system. *Quarterly Journal of the Royal Meteorological Society*, 137(656), 553–597.
164. Xia, Y., Hu, Y., & Liu, J. (2020). Comparison of trends in the Hadley circulation between CMIP6 and CMIP5. *Science Bulletin*, 65(19), 1667–1674.
165. Grise, K. M., & Davis, S. M. (2020). Hadley cell expansion in CMIP6 models. *Atmospheric Chemistry and Physics*, 20(9), 5249–5268.
166. Grise, K. M., Davis, S. M., Staten, P. W., & Adam, O. (2018). Regional and seasonal characteristics of the recent expansion of the tropics. *Journal of Climate*, 31(17), 6839–6856.
167. Grise, K. M., Davis, S. M., Simpson, I. R., Waugh, D. W., Fu, Q., Allen, R. J., Rosenlof, K. H., Ummenhofer, C. C., Karnauskas, K. B., Maycock, A. C., Quan, X.-W., Birner, T., & Staten, P. W. (2019). Recent tropical expansion: Natural variability or forced response? *Journal of Climate*, 32(5), 1551–1571.
168. Zaplotnik, Ž., Píkovnik, M., & Boljka, L. (2022). Recent Hadley circulation strengthening: A trend or multidecadal variability? *Journal of Climate*, 35(13), 4157–4176.
169. Allen, R. J., Sherwood, S. C., Norris, J. R., & Zender, C. S. (2012). Recent Northern Hemisphere tropical expansion primarily driven by black carbon and tropospheric ozone. *Nature*, 485(7398), 350–354.
170. Garfinkel, C. I., Waugh, D. W., & Polvani, L. M. (2015). Recent Hadley cell expansion: The role of internal atmospheric variability in reconciling modeled and observed trends. *Geophysical Research Letters*, 42(24), 10–824.
171. Allen, R. J., & Kovilakam, M. (2017). The role of natural climate variability in recent tropical expansion. *Journal of Climate*, 30(16), 6329–6350.
172. Mantsis, D. F., Sherwood, S., Allen, R., & Shi, L. (2017). Natural variations of tropical width and recent trends. *Geophysical Research Letters*, 44(8), 3825–3832.
173. Cheng, W., MacMartin, D. G., Kravitz, B., Visoni, D., Bednarz, E. M., Xu, Y., Luo, Y., Huang, L., Hu, Y., Staten, P. W., Hitchcock, P., Moore, J. C., Guo, A. -Ú., & Deng, X. (2022). Changes in Hadley circulation and intertropical convergence zone under strategic stratospheric aerosol geoengineering. *npj Climate and Atmospheric Science*, 5(1), 1–11.

174. Xia, Y., Wang, Y., Huang, Y., Hu, Y., Bian, J., Zhao, C., & Sun, C. (2021). Significant contribution of stratospheric water vapor to the poleward expansion of the Hadley circulation in autumn under greenhouse warming. *Geophysical Research Letters*, *48*(17), e2021GL094008.
175. Chemke, R., Polvani, L., & Deser, C. (2019). The effect of arctic sea ice loss on the Hadley circulation. *Geophysical Research Letters*, *46*(2), 963–972.
176. Tosca, M., Randerson, J., & Zender, C. (2013). Global impact of smoke aerosols from landscape fires on climate and the Hadley circulation. *Atmospheric Chemistry and Physics*, *13*(10), 5227–5241.
177. Bangalath, H. K., & Stenichikov, G. (2015). Role of dust direct radiative effect on the tropical rain belt over Middle East and North Africa: A high-resolution AGCM study. *Journal of Geophysical Research: Atmospheres*, *120*(10), 4564–4584.
178. Vecchi, G. A., & Soden, B. J. (2007). Global warming and the weakening of the tropical circulation. *Journal of Climate*, *20*(17), 4316–4340.
179. Sun, L., Chen, G., & Lu, J. (2013). Sensitivities and mechanisms of the zonal mean atmospheric circulation response to tropical warming. *Journal of the Atmospheric Sciences*, *70*(8), 2487–2504.
180. Tandon, N. F., Gerber, E. P., Sobel, A. H., & Polvani, L. M. (2013). Understanding Hadley cell expansion versus contraction: Insights from simplified models and implications for recent observations. *Journal of Climate*, *26*(12), 4304–4321.
181. Watt-Meyer, O., Frierson, D. M., & Fu, Q. (2019). Hemispheric asymmetry of tropical expansion under CO<sub>2</sub> forcing. *Geophysical Research Letters*, *46*(15), 9231–9240.
182. Gerber, E. P., & Son, S.-W. (2014). Quantifying the summertime response of the austral jet stream and Hadley cell to stratospheric ozone and greenhouse gases. *Journal of Climate*, *27*(14), 5538–5559.
183. Tao, L., Hu, Y., & Liu, J. (2016). Anthropogenic forcing on the Hadley circulation in CMIP5 simulations. *Climate Dynamics*, *46*(9–10), 3337–3350.
184. Polvani, L. M., Previdi, M., & Deser, C. (2011). Large cancellation, due to ozone recovery, of future Southern Hemisphere atmospheric circulation trends. *Geophysical Research Letters*, *38*(4), L04707.
185. Previdi, M., & Polvani, L. M. (2014). Climate system response to stratospheric ozone depletion and recovery. *Quarterly Journal of the Royal Meteorological Society*, *140*(685), 2401–2419.
186. Son, S.-W., Polvani, L. M., Waugh, D. W., Akiyoshi, H., Garcia, R., Kinnison, D., Pawson, S., Rozanov, E., Shepherd, T. G., & Shibata, K. (2008). The impact of stratospheric ozone recovery on the Southern Hemisphere westerly jet. *Science*, *320*(5882), 1486–1489.
187. Son, S.-W., Polvani, L. M., Waugh, D. W., Birner, T., Akiyoshi, H., Garcia, R. R., Gettelman, A., Plummer, D. A., & Rozanov, E. (2009). The impact of stratospheric ozone recovery on tropopause height trends. *Journal of Climate*, *22*(2), 429–445.
188. Son, S.-W., Gerber, E. P., Perlwitz, J., Polvani, L. M., Gillett, N., Seo, K.-H., Eyring, V., Shepherd, T. G., Waugh, D., Akiyoshi, H., Austin, J., Baumgaertner, A., Bekki, S., Braesicke, P., Brühl, C., Butchart, N., Chipperfield, M. P., Cugnet, D., Dameris, M., ... Yamashita, Y. (2010). Impact of stratospheric ozone on Southern Hemisphere circulation change: A multimodel assessment. *Journal of Geophysical Research*, *115*(D3), D00M07.
189. Polvani, L. M., Waugh, D. W., Correa, G. J. P., & Son, S.-W. (2011). Stratospheric ozone depletion: The main driver of twentieth-century atmospheric circulation changes in the Southern Hemisphere. *Journal of Climate*, *24*(3), 795–812.
190. Kang, S. M., Polvani, L., Fyfe, J., & Sigmond, M. (2011). Impact of polar ozone depletion on subtropical precipitation. *Science*, *332*(6032), 951–954.
191. Min, S.-K., & Son, S.-W. (2013). Multimodel attribution of the Southern Hemisphere Hadley cell widening: Major role of ozone depletion. *Journal of Geophysical Research: Atmospheres*, *118*(7), 3007–3015.
192. Hu, D., Guan, Z., & Tian, W. (2019). Signatures of the arctic stratospheric ozone in northern Hadley circulation extent and subtropical precipitation. *Geophysical Research Letters*, *46*(21), 12340–12349.
193. Banerjee, A., Fyfe, J. C., Polvani, L. M., Waugh, D., & Chang, K.-L. (2020). A pause in Southern Hemisphere circulation trends due to the Montreal Protocol. *Nature*, *579*(7800), 544–548.
194. Charlson, R. J., Langner, J., Rodhe, H., Leovy, C., & Warren, S. (1991). Perturbation of the Northern Hemisphere radiative balance by backscattering from anthropogenic sulfate aerosols. *Tellus A: Dynamic Meteorology and Oceanography*, *43*(4), 152–163.
195. Charlson, R. J., Schwartz, S., Hales, J., Cess, R. D., Coakley, J. J., Hansen, J., & Hofmann, D. (1992). Climate forcing by anthropogenic aerosols. *Science*, *255*(5043), 423–430.
196. Wang, H., Xie, S.-P., & Liu, Q. (2016). Comparison of climate response to anthropogenic aerosol versus greenhouse gas forcing: Distinct patterns. *Journal of Climate*, *29*(14), 5175–5188.
197. Wang, H., Xie, S.-P., Tokinaga, H., Liu, Q., & Kosaka, Y. (2016). Detecting cross-equatorial wind change as a fingerprint of climate response to anthropogenic aerosol forcing. *Geophysical Research Letters*, *43*(7), 3444–3450.
198. Wang, C.-C., Lee, W.-L., & Chou, C. (2019). Climate effects of anthropogenic aerosol forcing on tropical precipitation and circulations. *Journal of Climate*, *32*(16), 5275–5287.
199. Voigt, A., Pincus, R., Stevens, B., Bony, S., Boucher, O., Bellouin, N., Lewinschal, A., Medeiros, B., Wang, Z., & Zhang, H. (2017). Fast and slow shifts of the zonal-mean intertropical convergence zone in response to an idealized anthropogenic aerosol. *Journal of Advances in Modeling Earth Systems*, *9*(2), 870–892.
200. Wang, H., Xie, S.-P., Zheng, X.-T., Kosaka, Y., Xu, Y., & Geng, Y.-F. (2020). Dynamics of Southern Hemisphere atmospheric circulation response to anthropogenic aerosol forcing. *Geophysical Research Letters*, *47*(19), e2020GL089919.
201. Rotstayn, L., Collier, M. A., Jeffrey, S. J., Kidston, J., Syktus, J., & Wong, K. (2013). Anthropogenic effects on the subtropical jet in the Southern Hemisphere: Aerosols versus long-lived greenhouse gases. *Environmental Research Letters*, *8*(1), 014030.
202. Allen, R. J., & Ajoku, O. (2016). Future aerosol reductions and widening of the northern tropical belt. *Journal of Geophysical Research: Atmospheres*, *121*(12), 6765–6786.
203. Choi, J., Son, S.-W., & Park, R. J. (2019). Aerosol versus greenhouse gas impacts on Southern Hemisphere general circulation changes. *Climate Dynamics*, *52*, 4127–4142.
204. Steptoe, H., Wilcox, L., & Highwood, E. (2016). Is there a robust effect of anthropogenic aerosols on the southern annular mode? *Journal of Geophysical Research: Atmospheres*, *121*(17), 10–029.
205. Held, I. M., & Soden, B. J. (2006). Robust responses of the hydrological cycle to global warming. *Journal of Climate*, *19*(21), 5686–5699.
206. Griffiths, P. T., Murray, L. T., Zeng, G., Shin, Y. M., Abraham, N. L., Archibald, A. T., Deushi, M., Emmons, L. K., Galbally, I. E., Hassler, B., Horowitz, L. W., Keeble, J., Liu, J., Moehni, O., Naik, V., O'Connor, F. M., Oshima, N., Tarasick, D., Tilmes, S., ... Zanis, P. (2021). Tropospheric ozone in CMIP6 simulations. *Atmospheric Chemistry and Physics*, *21*(5), 4187–4218.
207. Ramanathan, V., & Carmichael, G. (2008). Global and regional climate changes due to black carbon. *Nature Geoscience*, *1*, 221–227.
208. Allen, R., Sherwood, S., Norris, J., & Zender, C. (2012). The equilibrium response to idealized thermal forcings in a comprehensive GCM: Implications for recent tropical expansion. *Atmospheric Chemistry and Physics*, *12*(10), 4795–4816.
209. Lacis, A., Hansen, J., & Sato, M. (1992). Climate forcing by stratospheric aerosols. *Geophysical Research Letters*, *19*(15), 1607–1610.
210. Haywood, J. M., Jones, A., Bellouin, N., & Stephenson, D. (2013). Asymmetric forcing from stratospheric aerosols impacts Sahelian rainfall. *Nature Climate Change*, *3*(7), 660–665.

211. Pausata, F. S. R., Chafik, L., Caballero, R., & Battisti, D. S. (2015). Impacts of high-latitude volcanic eruptions on ENSO and AMOC. *Proceedings of the National Academy of Sciences of the USA*, 112(45), 13784–13788.
212. Dogar, M. M. (2018). Impact of tropical volcanic eruptions on Hadley circulation using a high-resolution AGCM. *Current Science*, 114(6), 1284–1294.
213. Pausata, F. S. R., Zanchettin, D., Karamperidou, C., Caballero, R., & Battisti, D. S. (2020). ITCZ shift and extratropical teleconnections drive ENSO response to volcanic eruptions. *Science Advances*, 6(23), eaaz5006.
214. D'Agostino, R., & Timmreck, C. (2022). Sensitivity of regional monsoons to idealised equatorial volcanic eruption of different sulfur emission strengths. *Environmental Research Letters*, 17(5), 054001.
215. Man, W., Zhou, T., & Jungclaus, J. H. (2014). Effects of large volcanic eruptions on global summer climate and East Asian monsoon changes during the last millennium: Analysis of MPI-ESM simulations. *Journal of Climate*, 27(19), 7394–7409.
216. Iles, C. E., & Hegerl, G. C. (2014). The global precipitation response to volcanic eruptions in the CMIP5 models. *Environmental Research Letters*, 9(10), 104012.
217. Iles, C. E., & Hegerl, G. C. (2015). Systematic change in global patterns of streamflow following volcanic eruptions. *Nature Geoscience*, 8(11), 838–842.
218. Dogar, M. M., & Sato, T. (2019). Regional climate response of Middle Eastern, African, and South Asian monsoon regions to explosive volcanism and ENSO forcing. *Journal of Geophysical Research: Atmospheres*, 124(14), 7580–7598.
219. Colose, C. M., LeGrande, A. N., & Vuille, M. (2016). Hemispherically asymmetric volcanic forcing of tropical hydroclimate during the last millennium. *Earth System Dynamics*, 7(3), 681–696.
220. Liu, F., Chai, J., Wang, B., Liu, J., Zhang, X., & Wang, Z. (2016). Global monsoon precipitation responses to large volcanic eruptions. *Scientific Reports*, 6(1), 1–11.
221. Alfaro-Sánchez, R., Nguyen, H., Klesse, S., Hudson, A., Belmecheri, S., Köse, N., Diaz, H., Monson, R., Villalba, R., & Trouet, V. (2018). Climatic and volcanic forcing of tropical belt northern boundary over the past 800 years. *Nature Geoscience*, 11(12), 933–938.
222. Miller, R. L., Knippertz, P., García-Pando, C. P., Perlwitz, J. P., & Tegen, I. (2014). Impact of dust radiative forcing upon climate. In P. Knippertz & J. B. Stuut (Eds.) *Mineral Dust* (pp. 327–357). Springer.
223. Albani, S., & Mahowald, N. M. (2019). Paleodust insights into dust impacts on climate. *Journal of Climate*, 32(22), 7897–7913.
224. Zanchettin, D., Timmreck, C., Khodri, M., Schmidt, A., Toohey, M., Abe, M., Bekki, S., Cole, J., Fang, S.-W., Feng, W., Hegerl, G., Johnson, B., Lebas, N., LeGrande, A. N., Mann, G. W., Marshall, L., Rieger, L., Robock, A., Rubinetti, S., ... Weierbach, H. (2021). Effects of forcing differences and initial conditions on inter-model agreement in the volmpic volc-pinatubo-full experiment. *Geoscientific Model Development Discussions*, 15, 2265–2292.
225. Paillard, D., & Parrenin, F. (2004). The Antarctic ice sheet and the triggering of deglaciations. *Earth and Planetary Science Letters*, 227(3–4), 263–271.
226. Tziperman, E., Raymo, M. E., Huybers, P., & Wunsch, C. (2006). Consequences of pacing the Pleistocene 100 kyr ice ages by non-linear phase locking to Milankovitch forcing. *Paleoceanography and Paleoclimatology*, 21(4), PA4206.
227. Milankovitch, M. (1941). Canon of insolation and the iceage problem. *Koniglich Serbische Akademie Beograd Special Publication*, 132.
228. Hays, J. D., Imbrie, J., & Shackleton, N. J. (1976). Variations in the Earth's orbit: Pacemaker of the ice ages: For 500,000 years, major climatic changes have followed variations in obliquity and precession. *Science*, 194(4270), 1121–1132.
229. Berger, A. (1988). Milankovitch theory and climate. *Reviews of Geophysics*, 26(4), 624–657.
230. Khon, V., Park, W., Latif, M., Mokhov, I. I., & Schneider, B. (2012). Tropical circulation and hydrological cycle response to orbital forcing. *Geophysical Research Letters*, 39(15), L15708.
231. Jaliha, C., Srinivasan, J., & Chakraborty, A. (2019). Modulation of Indian monsoon by water vapor and cloud feedback over the past 22,000 years. *Nature Communications*, 10(1), 1–8.
232. D'Agostino, R., Brown, J. R., Moise, A., Nguyen, H., Dias, P. L. S., & Jungclaus, J. (2020). Contrasting Southern Hemisphere monsoon response: MidHolocene orbital forcing versus future greenhouse gas-induced global warming. *Journal of Climate*, 33(22), 9595–9613.
233. Wang, T., Wang, N., & Jiang, D. (2023). Last glacial maximum ITCZ changes from PMIP3/4 simulations. *Journal of Geophysical Research: Atmospheres*, 128(10), e2022JD038103.
234. Ganopolski, A., & Brovkin, V. (2017). Simulation of climate, ice sheets and CO<sub>2</sub> evolution during the last four glacial cycles with an earth system model of intermediate complexity. *Climate of the Past*, 13(12), 1695–1716.
235. Ferreira, D., Marshall, J., Ito, T., & McGee, D. (2018). Linking glacial-interglacial states to multiple equilibria of climate. *Geophysical Research Letters*, 45(17), 9160–9170.
236. McGee, D., Moreno-Chamarro, E., Green, B., Marshall, J., Galbraith, E., & Bradtmiller, L. (2018). Hemispherically asymmetric trade wind changes as signatures of past ITCZ shifts. *Quaternary Science Reviews*, 180, 214–228.
237. Otto-Bliesner, B. L., & Clement, A. (2004). The sensitivity of the Hadley circulation to past and future forcings in two climate models. In H. F. Diaz & R. S. Bradley (Eds.), *The Hadley circulation: Present, past and future* (pp. 437–464). Springer.
238. Hoskins, B. J., Yang, G., & Fonseca, R. M. (2020). The detailed dynamics of the June–August Hadley cell. *Quarterly Journal of the Royal Meteorological Society*, 146, 557–575.
239. Hoskins, B. J., & Yang, G. (2021). The detailed dynamics of the Hadley cell. Part 2: December to February. *Journal of Climate*, 34(2), 805–823.
240. Hu, Y., Huang, H., & Zhou, C. (2018). Widening and weakening of the Hadley circulation under global warming. *Science Bulletin*, 63(10), 640–644.
241. Kaufman, Y., Tanré, D., Dubovik, O., Karnieli, A., & Remer, L. (2001). Absorption of sunlight by dust as inferred from satellite and ground-based remote sensing. *Geophysical Research Letters*, 28(8), 1479–1482.
242. Yoshioka, M., Mahowald, N. M., Conley, A. J., Collins, W. D., Fillmore, D. W., Zender, C. S., & Coleman, D. B. (2007). Impact of desert dust radiative forcing on Sahel precipitation: Relative importance of dust compared to sea surface temperature variations, vegetation changes, and greenhouse gas warming. *Journal of Climate*, 20(8), 1445–1467.
243. Lau, K., Kim, K., Sud, Y., & Walker, G. (2009). A GCM study of the response of the atmospheric water cycle of West Africa and the Atlantic to Saharan dust radiative forcing. *Annales Geophysicae*, 27, 4023–4037.
244. Yue, X., Liao, H., Wang, H., Li, S., & Tang, J. (2011). Role of sea surface temperature responses in simulation of the climatic effect of mineral dust aerosol. *Atmospheric Chemistry and Physics*, 11(12), 6049–6062.
245. Yue, X., Wang, H., Liao, H., & Jiang, D. (2011). Simulation of the direct radiative effect of mineral dust aerosol on the climate at the last glacial maximum. *Journal of Climate*, 24(3), 843–858.
246. Pausata, F. S. R., Messori, G., & Zhang, Q. (2016). Impacts of dust reduction on the northward expansion of the African monsoon during the Green Sahara period. *Earth and Planetary Science Letters*, 434, 298–307.
247. Mamalakis, A., Randerson, J. T., Yu, J.-Y., Pritchard, M. S., Magnusdottir, G., Smyth, P., Levine, P. A., Yu, S., & Fofoula-Georgiou, E. (2021). Zonally contrasting shifts of the tropical rain belt in response to climate change. *Nature Climate Change*, 11(2), 143–151.

248. Pascale, S., Carvalho, L. M. V., Adams, D. K., Castro, C. L., & Cavalcanti, I. F. A. (2019). Current and future variations of the monsoons of the Americas in a warming climate. *Current Climate Change Reports*, 5, 125–144.
249. Dunning, C. M., Black, E., & Allan, R. P. (2018). Later wet seasons with more intense rainfall over Africa under future climate change. *Journal of Climate*, 31, 9719–9738.
250. Kang, S. M., Deser, C., & Polvani, L. M. (2013). Uncertainty in climate change projections of the Hadley circulation: The role of internal variability. *Journal of Climate*, 26(19), 7541–7554.
251. Lau, W. K., & Kim, K.-M. (2015). Robust Hadley circulation changes and increasing global dryness due to CO<sub>2</sub> warming from CMIP5 model projections. *Proceedings of the National Academy of Sciences*, 112, 3630–3635.
252. Hu, Y., Zhou, C., & Liu, J. (2011). Observational evidence for poleward expansion of the Hadley circulation. *Advances in Atmospheric Sciences*, 28(1), 33–44.
253. Chemke, R., & Yuval, J. (2023). Human-induced weakening of the Northern Hemisphere tropical circulation. *Nature*, 617, 529–532.

**How to cite this article:** Lionello, P., D'Agostino, R., Ferreira, D., Nguyen, H., & Singh, M. S. (2024). The Hadley circulation in a changing climate. *Ann NY Acad Sci.*, 1534, 69–93.  
<https://doi.org/10.1111/nyas.15114>